ChemComm

ROYAL SOCIETY OF CHEMISTRY

FEATURE ARTICLE

View Article Online
View Journal | View Issue

Cite this: *Chem. Commun.*, 2025, **61**, 9836

Recent advances in functionalized cycloparaphenylenes: from molecular design to applications

Xiaonan Li,† Shengzhu Guo† and Hua Jiang *

Received 24th April 2025,
Accepted 4th June 2025

DOI: 10.1039/d5cc02286j

rsc.li/chemcomm

Cycloparaphenylenes (CPPs), which feature a radial π-system, have attracted considerable attention due to their size-dependent photophysical properties and distinctive curved π-conjugated cavity. Incorporating aromatic systems beyond benzene enables precise tuning of their optoelectronic properties to meet specific requirements in supramolecular chemistry and materials science. In this review, we systematically summarize the synthesis, properties, and functional applications of CPP derivatives in chiral materials, supramolecular chemistry, and photoelectric devices. It is anticipated that this review will provide valuable insights for researchers working on CPP derivatives and carbon nanohoops, and contribute to the advancement of synthetic chemistry and materials chemistry.

1. Introduction

The pursuit of novel carbon allotropes with atomic precision has driven substantial advancements in the field of carbon nanotechnology.[1–4] From fullerenes[5–8] and carbon nanotubes (CNTs) to graphene[9] and cycloparaphenylenes (CPPs),[10,11] each new form of carbon has not only expanded our understanding of its versatility but also unlocked new possibilities for functional materials (Fig. 1). As researchers delve deeper into the synthesis, functionalization, and assembly of carbon nanostructures, the potential applications of these materials in electronics, energy storage, catalysis, and biomedicine are expected to proliferate. The future of carbon nanotechnology hinges on achieving precise synthesis of topological carbon materials and developing sustainable methodologies for their production, thereby paving the way for next-generation technologies and innovative solutions to global challenges.

As prominent representatives of carbon materials, CPPs, which were first conceptualized in theoretical studies as the shortest possible segments of armchair CNTs, have garnered significant attention in the fields of organic chemistry, supramolecular chemistry, and materials science.[12–15] However, their synthesis remained elusive for decades due to the strain and conformational challenges of macrocyclization. The breakthrough came in 2008 when Jasti, Bertozzi, and coworkers[10]

College of Chemistry, Beijing Normal University, Beijing 100875, P.R. China. E-mail: jiangh@bnu.edu.cn

† These authors contributed equally to this work.

Xiaonan Li

Xiaonan Li received her master's degree in organic chemistry from Beijing Normal University in 2023 and is currently pursuing a PhD under the supervision of Professor Hua Jiang. Her research focuses on supramolecular organic chemistry, particularly the design and synthesis of novel π-conjugated macrocycles, and explores their potential applications in host–guest chemistry and supramolecular functional materials.

Shengzhu Guo

Shengzhu Guo received his master's degree in chemical engineering and technology from Wuyi University in 2022 and subsequently relocated to Beijing Normal University to embark on a PhD specializing in organic chemistry under the guidance of Professor Hua Jiang. Currently, his research focuses on the development of synthetic methodologies for π-conjugated macrocycles and their applications in host–guest chemistry and supramolecular systems.

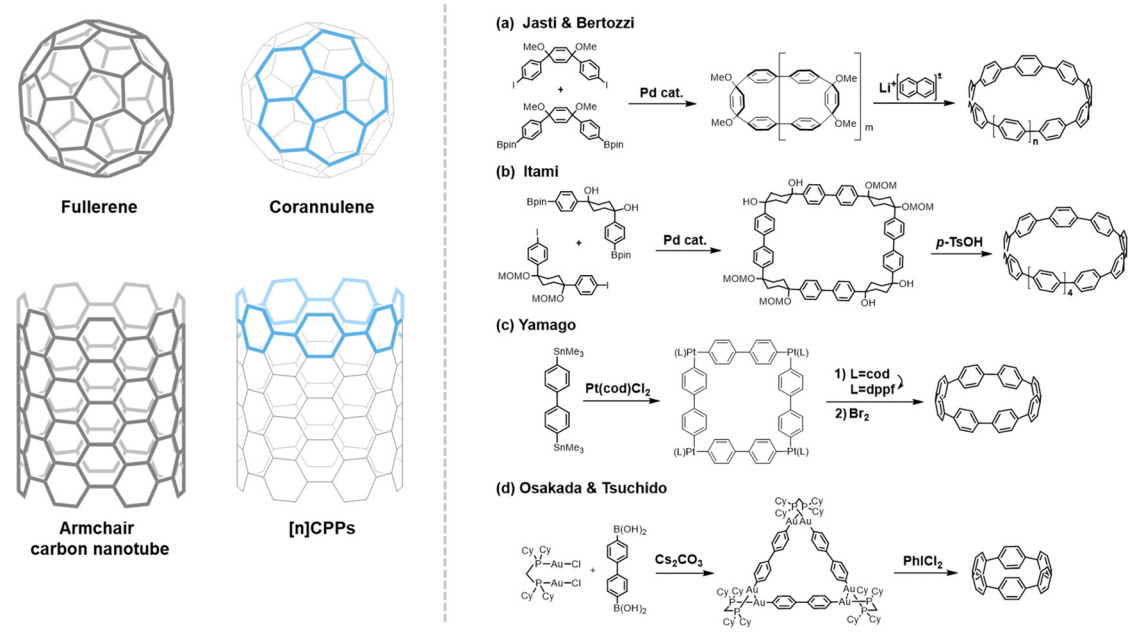

Fig. 1 Structures of carbon allotropes and (a–d) the synthetic procedures of [*n*]CPPs.

reported the first synthesis of [9]-, [12]-, and [18]CPP *via* a stepwise, reductive aromatization strategy (Fig. 1a). This landmark work unlocked access to these strained, radially π-conjugated systems. Subsequent synthetic advances were achieved by Yamago,[16] Itami,[17] Osakada and Tsuchido[18] through several alternative routes, including platinum-mediated cyclization, iterative Suzuki–Miyaura couplings and gold-mediated cyclization (Fig. 1b–d). The versatility of [*n*]CPPs is further enhanced by their potential as building blocks for developing structurally diverse conjugated carbon nanohoops. This can be achieved through the strategic incorporation of aromatic systems beyond benzene, enabling precise tuning of their optoelectronic properties to meet specific requirements in supramolecular chemistry and materials science.

Recent years have witnessed a surge in research exploring the exceptional properties of CPPs and their derivatives, accompanied by several comprehensive reviews documenting these advancements. Thus, in this review, we will focus on the recent advances in the synthesis and applications of novel CPP derivatives that have emerged in the last decade. Herein, we provide a comprehensive analysis of recent progress in the design, synthesis, and application of these topologically unique molecules, emphasizing their potential to contribute significantly to future organic functional material developments. We anticipate that this review will be a guiding source for the development of supramolecular chemistry and materials chemistry.

Hua Jiang

Hua Jiang, a Professor at Beijing Normal University, completed his undergraduate studies at Hubei University in 1991 and subsequently worked there as an assistant engineer until 1995. He received his master's degree in organic chemistry in 1998 at Wuhan University, and PhD in organic chemistry in 2001 at the Institute of Chemistry, Chinese Academy of Sciences (ICCAS). Subsequently, he was a post-doctoral fellow at the Institut Européen de Chimieet Biologie (France) and University of Notre Dame (USA). In 2006, he joined ICCAS as a Professor and then moved to Beijing Normal University in 2013. He is actively engaged in the study of the synthesis of organic functionalized molecules and supramolecular chemistry, focusing on the development of novel chiral organic supramolecular systems including helical foldamers, π-conjugated nanocarbon molecules, mechanical interlocking molecules, and molecular machines.

2. Chiral CPP derivatives and their applications in advanced chiral materials

Chirality occupies a pivotal position in various scientific and technological domains, including molecular synthesis, materials design, enantioselective catalysis, fundamental physics, pharmaceutics, and biomedicine.[19–22] Chiral [*n*]CPP derivatives have garnered significant attention due to their unique chiroptical properties, which make them highly promising for applications in 3D displays, security encryption, asymmetric synthesis, and circularly polarized luminescence (CPL) materials. As a result, several chiral CPP derivatives have been

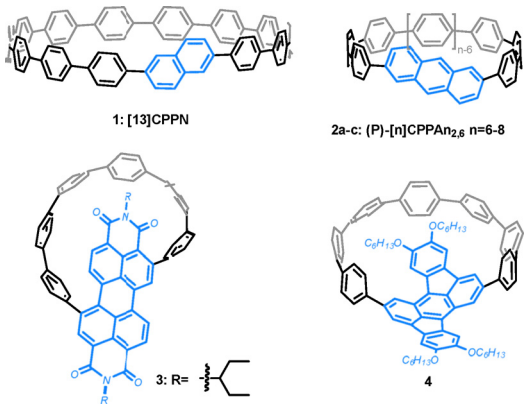

Fig. 2 Structures of chiral CPP-derivates **1–4**.

reported, exhibiting remarkable performance in chiral materials and further expanding the diversity of CPL materials. A promising strategy to construct chiral CPP derivatives is to fabricate achiral functional groups into the CPP framework. This modification breaks the structural symmetry of the nanohoop by introducing conformational bending, strain, and steric hindrance, thereby endowing the system with distinct chiral properties. For example, the incorporation of achiral aromatic units, such as naphthalene[23] and 2,6-anthrylene,[24] into the CPP backbone generates chiral CPP analogs (**1** and **2**, shown in Fig. 2), which can be regarded as the shortest chiral single-walled carbon nanotubes (SWCNTs) exhibiting helical chirality. Meanwhile, nanohoops **2** confirms that inherent chirality is more pronounced in smaller ring sizes. Accordingly, planar achiral moieties like perylene diimide (PDI) and rubicene, when embedded into the strained CPP framework, nanohoops **3**[25] and **4**[26] undergo structural symmetry breaking due to torsional distortion, resulting in pronounced chiral characteristics. However, some of the chiral nanohoops synthesized by inserting an achiral functional group undergoes rapid racemization at ambient temperature, thereby limiting their further application in chiral materials.[23]

Incorporating chiral moieties into the framework of [*n*]CPPs enables precise control over the chiral properties of the resulting molecules, thereby facilitating the development of customized materials tailored for specific applications. Chiral binaphthyl molecules have been extensively studied in the field of chiral materials and serve as crucial building blocks for the construction of carbon macrocycles (Fig. 3). In 2020, Mazaki[27] and coworkers synthesized nanohoop **5**, which is directly linked to the framework of CPP at the 7,7′-position of binaphthyl and can serve as a solid-state CPL dye. Du *et al.* subsequently reported the synthesis of chiral binaphthyl nanohoops **6**[28] and **7**,[29] connected the skeleton of CPP at the 3,3′- and 1,1′-positions of binaphthyl respectively, for CPL studies. Furthermore, Tanaka[30] also reported the use of sterically demanding binaphthyl-linked diyne as a chiral functional group for the synthesis of chiral nanohoop **8**. These studies demonstrate that incorporating a chiral binaphthyl scaffold into a macrocyclic structure at varying positions results in distinct properties.

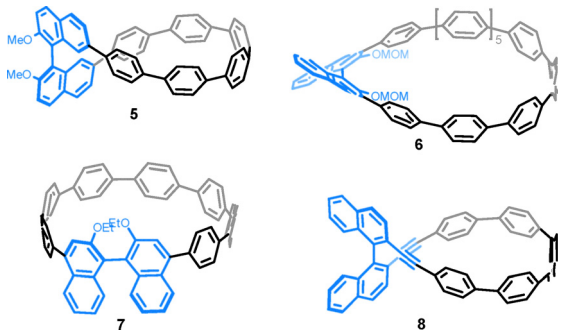

Fig. 3 Structures of binaphthyl-based chiral CPP-derivates **5–8**.

[2.2]Paracyclophane can also serve as essential building blocks for the construction of carbon macrocycles. In 2022, our group[31] achieved the successful synthesis of chiral [2.2]PCP-based nanohoops **9** (PCP-[*n*]CPP) by incorporating a functionalized pseudo *meta*-[2.2]PCP unit with CPP backbones of varying dimensions (Fig. 4). The structural integrity of the nanohoops was validated through X-ray crystallographic analysis, and they demonstrate size-dependent crystal packing patterns. Meanwhile, the macrocycles exhibit intriguing size-dependent UV-vis absorption and fluorescence emission properties, characterized by exceptionally high quantum yields of up to 0.82 and favourable chiroptical properties with dissymmetry factors on the order of 10^{-3}. The study also highlights the importance of chirality transfer and structural design in achieving stable and functional chiral macrocycles.

Next, our group[32] reported the regioselective synthesis of all-carbon lemniscular nanohoops, **10a** (*bis-po*-CC) and **10b** (*bis-pm*-CC), through strategic control of ring closures at distinct positions of planar chiral tetrasubstituted[2.2]PCP (Fig. 5).

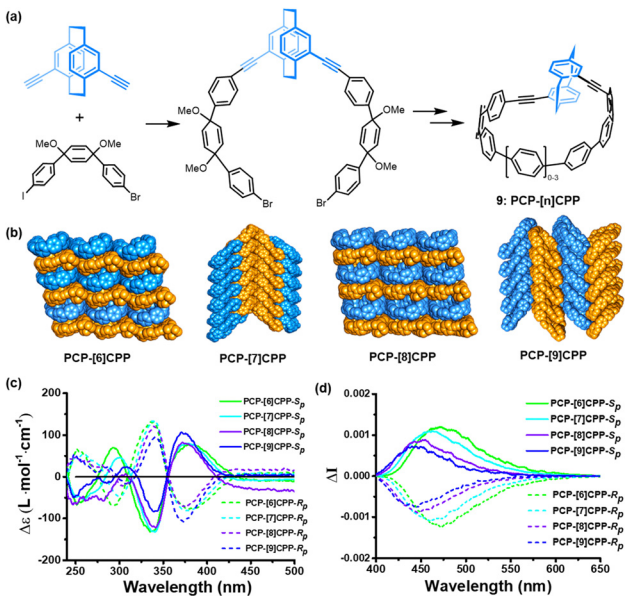

Fig. 4 The (a) synthetic procedures, (b) dense stack (c) CD and (d) CPL spectra of compound **9**. Adapted from ref. 31 with permission from Wiley-VCH, copyright 2022.

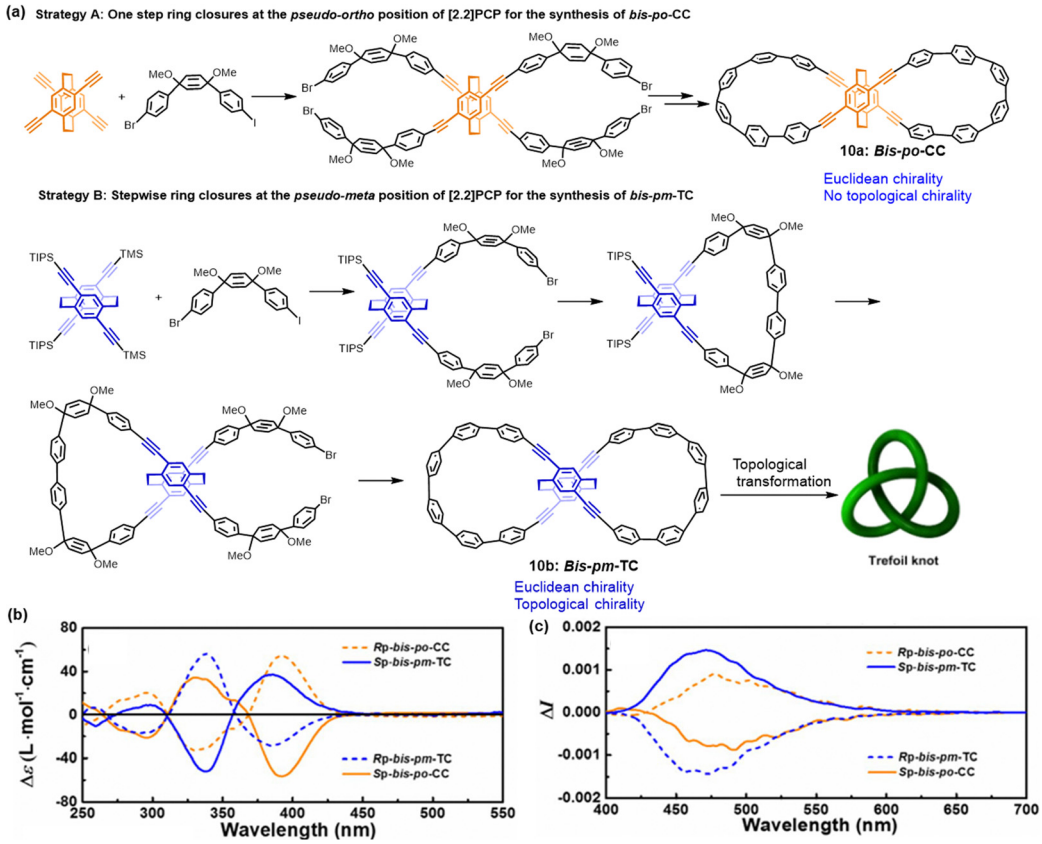

Fig. 5 (a) Regioselective synthesis of isomers **10** with a differently oriented [2.2]PCP core in which ethylene bridges are located out of and in the lemniscular framework, respectively. (b) CD and (c) CPL spectra of compound **10**. Adapted from ref. 32 with permission from Royal Society of Chemistry, copyright 2023.

Topological analyses demonstrated that **10b** features a nonplanar trefoil graph, while **10a** shows a planar graph, and consequently, **10b** exhibits topological chirality, while **10a** is topologically achiral. CD and CPL measurements demonstrated that the chiroptical properties of **10b** differ markedly from those of **10a**. The CD spectra of **10b** showed an inverted sign

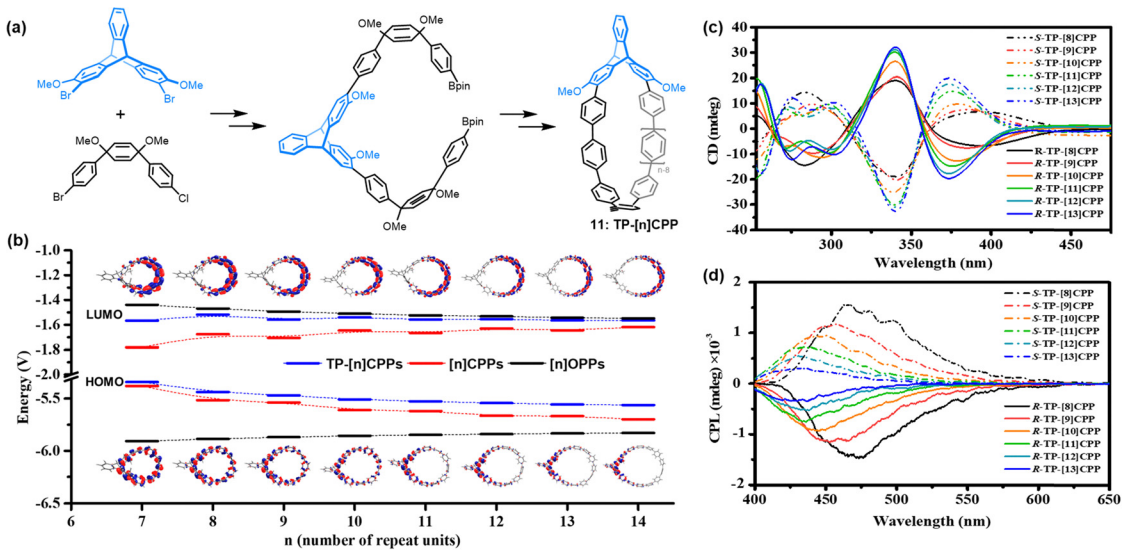

Fig. 6 (a) Synthetic procedures of chiral triptycene-based nanohoops **11**, (b) the frontier molecular orbitals and LUMO–HOMO gaps for TP-[*n*]CPPs, [*n*]CPPs, and [*n*]OPPs at the optimized geometries of S_0 state calculated by DFT at the PBE0/6-31G(d)/PCM level, (c) CD and (d) CPL spectra of macrocycles **11** in DCM solution (1.0×10^{-5} M); adapted from ref. 33 with permission from Wiley-VCH, copyright 2024.

compared to **10a**, indicating opposite chirality despite sharing the same planar chiral PCP core. CPL spectra further confirmed these findings, with **10b** displaying a negative signal in the range of 400–700 nm, consistent with the CD results. These differences are attributed to the distinct orientation of the embedded [2.2]PCP core within the lemniscular nanohoops and their differing topological chiralities. This study highlights the influence of regioselective synthesis on the topological chirality of these nanohoops, providing new insights into the design and synthesis of topologically chiral all-carbon molecules.

Very recently, our group[33] reported the rational design and synthesis of highly luminescent chiral triptycene-based nanohoops **11** (TP-[*n*]CPP) with broken symmetry by embedding chiral 2,6-dimethoxytriptycene into the frames of [*n*]CPPs (Fig. 6). The nanohoops exhibited unique size-dependent frontier molecular orbitals and consequently displayed size-dependent photophysical properties. This suggests that incorporating aromatic systems beyond benzene can effectively control the topologies of the frontier molecular orbitals, enabling precise tuning of their optoelectronic properties. Nanohoops **11** demonstrate exceptionally high fluorescence quantum yields, with TP-[13]CPP achieving a maximum value of 0.93. This represents the highest fluorescence quantum yield reported to date for chiral conjugated carbon nanohoops. The exceptional luminescence efficiency is attributed to the unique acyclic and radial conjugation within the nanohoops, as well as their elevated radiative transition rates, which were further validated through theoretical investigations. Chiroptical analyses revealed that these chiral TP-[*n*]CPPs exhibit intense CPL, with CPL brightness reaching up to 100.5 M^{-1} cm^{-1} for TP-[11]CPP. This high CPL brightness is directly correlated with the high fluorescence quantum yields of the nanohoops. Notably, the studies uncovered an intriguing size-dependent relationship in the (chir)optical properties of Nanohoops **11**, which exhibits a linear trend when plotted against $1/n$ (where n denotes the number of repeating units). This linear correlation offers profound insights into the structural and electronic factors influencing the optical and chiroptical behaviors of these nanohoops.

Other chiral building blocks, such as stereogenic Tröger's base,[34] [6]helicene[35] and [5]helicene,[36] when incorporated into CPP architectures, have facilitated the development of chiral CPP analogs **12–14** (as depicted in Fig. 7). These nanohoops demonstrate remarkable (chiro)optical properties, with dissymmetry factors on the order of 10^{-3}, positioning them as highly promising candidates for applications in chiral optoelectronics and asymmetric synthesis. Furthermore, the identification of Möbius strip topology in nanohoops **13** and **14** highlights their potential as topological materials exhibiting unique electronic and optical characteristics.

In the pursuit of stable chiral nanostructures, researchers have explored the concept of writhe stabilization through cross-linking, as opposed to relying solely on twist to prevent unwinding. This approach has led to the development of axially chiral figure-eight CPPs, where the writhe is stabilized by

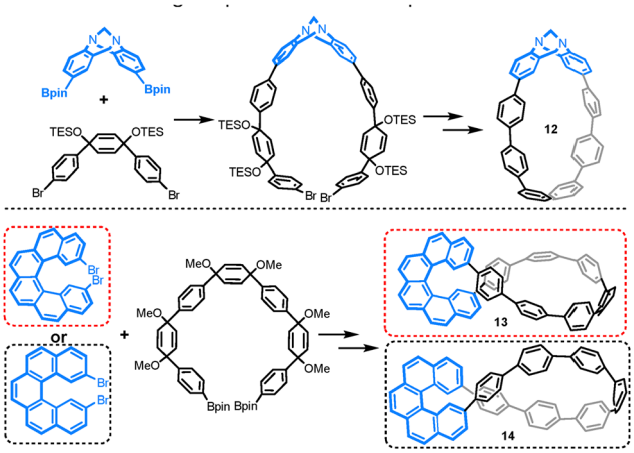

Fig. 7 The synthetic procedures of compounds **12–14**.

cross-linking, resulting in a robust three-dimensional structure. This strategy has proven particularly effective in maintaining the chiral integrity of the macrocycles, preventing racemization, and enhancing their chiroptical properties. To achieve this, three-dimensional building blocks such as bicarbazole,[37] spirobifluorene,[38] binaphthyl units[30] and 2,11,18,27-tetrabromooctabenzo[8]circulene[39] have been strategically incorporated as structural units in the synthesis of chiral cycloparaphenylene-based molecular lemniscates **15–18** (Fig. 8). These building blocks not only provide the necessary rigidity to stabilize the writhe but also introduce additional functional groups that enhance the overall stability and performance of the resulting macrocycles. These macrocycles exhibit pronounced CPL, with nanohoop **17** showing a high affinity for vapor analytes. This characteristic renders them highly valuable for applications in chiral sensing, optoelectronics, and chemical detection.

In 2019, Cong and coworkers described the synthesis of a pentiptycene-derived chiral dual nanohoop molecule **19**[40] with key steps including ring expansion through dianthracene cycloreversion and transannular [4+2] cycloaddition across a 64-membered macrocycle (Fig. 9). The crystal structure of the nanoring molecule exhibits an orderly stacking pattern and forms a long-range channel structure in the solid state. Furthermore, the nanoring enantiomers were successfully resolved, and the macrocycle demonstrates exceptional chiral properties, with $|g_{lum}|$ reaching the order of 10^{-3}. Subsequently, Du reported a novel chiral dual-emissive bismacrocycle **20**[41] with tunable aggregation-induced emission colors. This compound features a 1,2,4,5-tetraphenylbenzene core locked by two intersecting polyphenylene-based macrocycles. The luminescence behavior of **20** shows the unique characteristics of both the ACQ effect and AIE effect, inducing a remarkable redshift emission with near white-light emission. In addition, **20** displays enhanced circularly polarized luminescence properties due to the AIE effect.

In 2024, Cong[42] and coworkers reported the synthesis of helical tubular molecule **21** featuring three diyne linkers between two site-specifically functionalized [9]CPP (Fig. 10). This radially conjugated compound demonstrates remarkable solid-state packing patterns, exceptional CPL properties, and

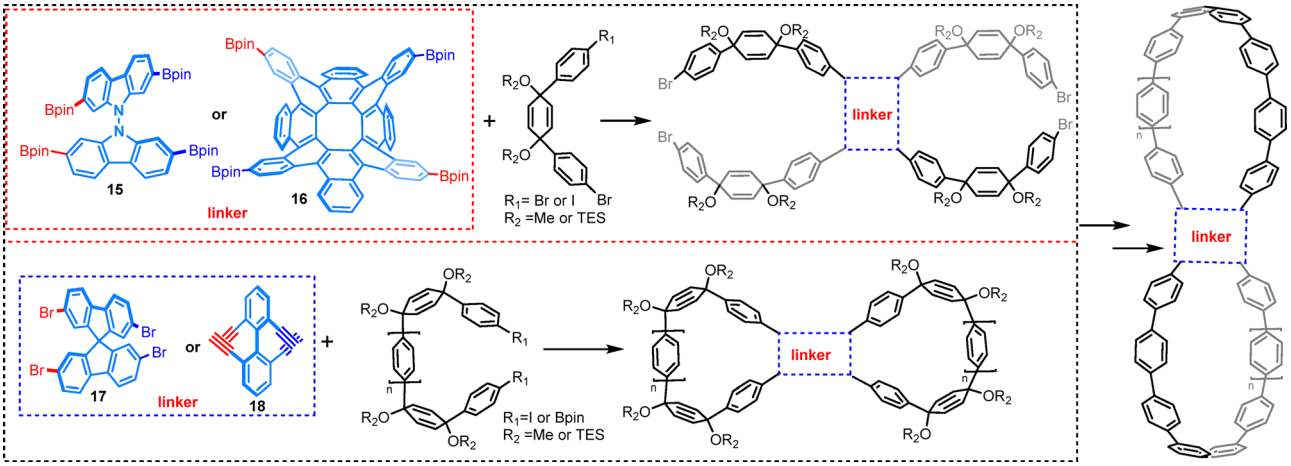

Fig. 8 Structures of chiral bis-nanohoops **15–18**.

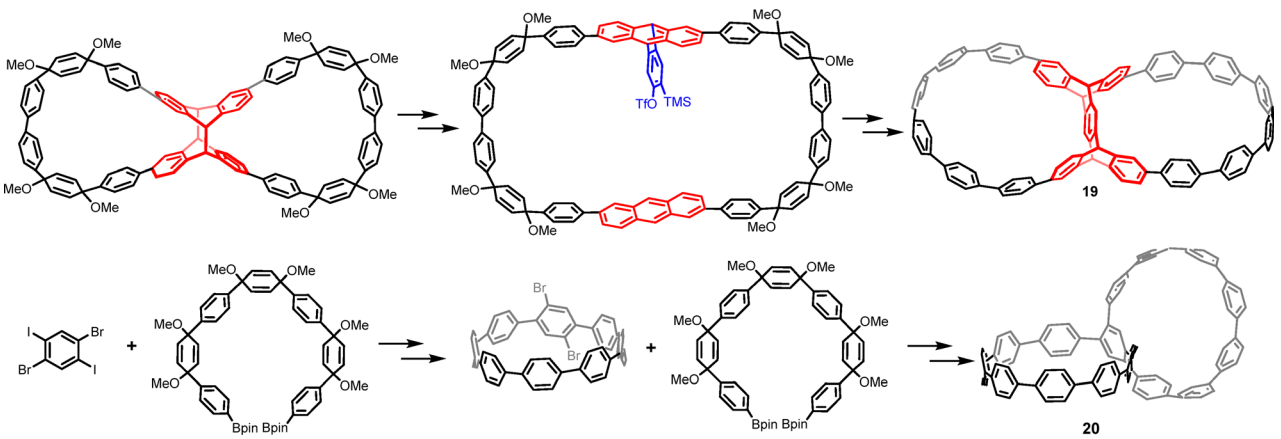

Fig. 9 The synthetic procedures of compounds **19** and **20**.

facile post-functionalization. In the solid state, the crystal structure of **21** displays a C_3-symmetrical packing mode with a trigonal $R\bar{3}c$ space group, wherein pairs of enantiomers alternate in a hexamer pattern featuring threefold rotation axes and one-dimensional channels along the [001] direction. Notably, **21** demonstrates outstanding chiroptical properties, with $|g_{lum}|$ reaching the order of 10^{-2}. This study is expected to inspire future bottom-up synthesis efforts aimed at creating a wider range of chiral tubular structures derived from CPPs, thus paving the way for the expansion of molecular nanocarbons with emergent properties.

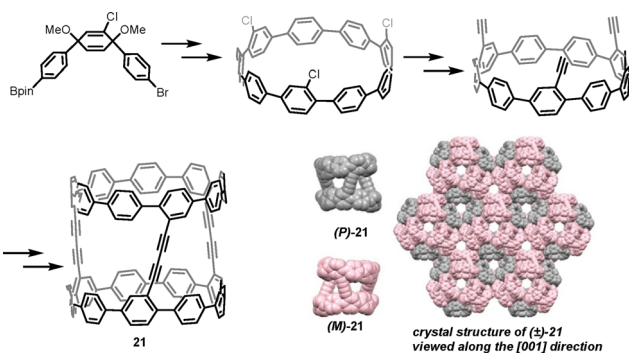

Fig. 10 (a) Structures of chiral CPP-derivates and (b) single crystals of **21**. Adapted from ref. 42 with permission from Wiley-VCH, copyright 2024.

3. Functionalized CPPs and their application in supramolecular chemistry

The unique curved π-surface structures and concave cavities of [*n*]CPPs enable them to function as effective hosts for both aromatic and nonaromatic guests with complementary curved surfaces through CH–π hydrogen bonds, π–π interactions, and dispersion forces, resulting in the formation of stable binary or ternary complexes.[43,44] We[45] have comprehensively summarized the most recent advances and examples on host–guest chemistry of binary and ternary complexes utilizing [*n*]CPPs and related derivatives. In this feature article, we highlight the application of CPP in supramolecular chemistry over the past

few years, with a focus on the precise control of molecular topologies.

In contrast to alternant hydrocarbons, the incorporation of nonalternant systems reduces the aromaticity of nanohoops, resulting in a narrower HOMO–LUMO energy gap and more pronounced changes in their optoelectronic properties. Azulene, a classic nonalternant aromatic hydrocarbon, is particularly notable for its ease of protonation, rendering it an ideal candidate for designing stimuli-responsive systems. These unique characteristics make it highly suitable for constructing stimuli-responsive nanohoops with potential applications in host–guest chemistry. In 2023, our group[46] reported the synthesis of a novel nonalternant azulene-embedded carbon nanohoop, **22a** (1,3-Az[9]CPP), which exhibits reversible pH stimuli-responsiveness, anti-Kasha emission, and tunable band gaps upon protonation and deprotonation (Fig. 11). The nanohoop demonstrated a significant shift in its UV-vis absorption spectra upon protonation, with the optical gap decreasing from 2.74 eV to 1.82 eV, indicating a strong modulation of electronic properties. Furthermore, the structural and binding properties were confirmed by single-crystal X-ray diffraction, revealing a 1 : 1 host–guest complex with C_{60}. And **22a** showed highly selective binding for C_{60} over C_{70} in acidic media, with a binding constant ratio $Ka_{C_{60}/C_{70}}$ = 30. This selectivity was attributed to the enhanced cation–π interactions between the protonated azulene unit and the fullerene.

In 2023, our group[47] reported the synthesis and chiroptical properties of novel chiral carbon nanoring **23** ([12]PCPP) containing a planar chiral [2.2]PCP unit (Fig. 12). Nanoring **23** demonstrates exceptional UV-vis absorption and fluorescence emission properties, characterized by exceptionally high quantum yields of up to 0.71 and favorable chiroptical properties with dissymmetry factors on the order of 10^{-3}. Meanwhile, we discovered that nanohoop **23** exhibits outstanding performance

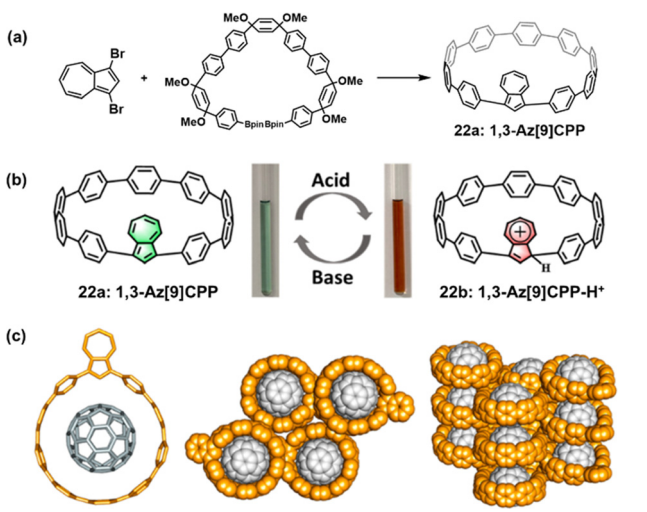

Fig. 11 The (a) synthetic procedure and (b) reversible pH stimuli-responsiveness of **22** and (c) X-ray crystal structures of C_{60}@**22a**. Adapted from ref. 46 with permission from Royal Society of Chemistry, copyright 2023.

in supramolecular chemistry, particularly in the construction of Russian doll complexes with 18-crown-6 and *S*/*R*-protonated amines. The homochiral *S@Sp*- and *R@Rp*-ternary complexes demonstrated a highly narcissistic chiral self-recognition for *S*/*R*-protonated chiral amines, respectively. This unique property underscores the ability of nanohoop **23** to selectively recognize and differentiate chiral guests based on their stereochemistry. The chiral ternary complexes formed by nanohoop **23** can be further applied to determine the enantiomeric excess (ee) values of chiral guests. This application highlights the potential of carbon nanorings in developing supramolecular sensors for chiral recognition and analysis, offering a new approach to determining the ee values of chiral molecules.

Furthermore, our group[48] reported the synthesis and characterization of heterotopic bisnanohoops **24** (P5-[8,10]CPPs) which integrate CPPs with a pillar[5]arene (P5A) unit (Fig. 13). These compounds exhibit remarkable chiral properties, characterized by $|g_{lum}|$ values on the order of 10^{-3}.[49] This value is comparable to that of C_5-symmetric P5A and significantly larger than those of previously reported CPL-active P5A compounds.[50] The latter were prepared *via* single-unit modification, which resulted in the loss of C_5-symmetry and exhibited $|g_{lum}|$ values on the order of 10^{-4}.[51–53] Meanwhile, nanohoop **24** demonstrate supramolecular chemical potential, particularly in the construction of sophisticated Förster resonance energy transfer (FRET) systems. Through host–guest interactions, these bisnanohoops can self-assemble with various acceptor molecules, such as BODIPY-Br and Rh–Br, which have distinct emission spectra. This self-assembly process enables the precise tuning of energy transfer between the donor (**24**) and the acceptors, facilitating multi-color tunable emissions, including white-light emission. The ability to achieve white-light emission through these FRET systems has significant practical implications. The host–guest complexes formed between **24** and the acceptor molecules have been successfully employed in the development of white-light fluorescent films. These films exhibit stable and efficient white-light emission, making them suitable for integration with 365 nm LED lamps to produce functional white LED devices. This integration represents a significant step forward in the application of chiral nanohoops in optoelectronic devices and lighting technologies.

Furthermore, our[54] investigations revealed that nanohoop **11** exhibits exceptional performance in supramolecular chemistry and has been employed to construct Russian-doll-like complexes with P5A and haloalkyl derivatives of 9,10-bis(phenylethynyl)anthracene (Fig. 14). Nanohoop **11** not only functions as a host for P5A but also serves as an energy donor in the construction of FRET systems. Importantly, we demonstrated that the hierarchical assembly processes could be efficiently monitored in real time using FRET. Notably, the Russian-doll complexes exhibited both one-step and sequential FRET behavior dependent on the subcomponents P5A/P5A-An during hierarchical assembly, reminiscent of the structure and energy transfer mechanisms observed in the light-harvesting systems of purple bacteria. These findings underscore the importance of matching the dimensions of two distinct

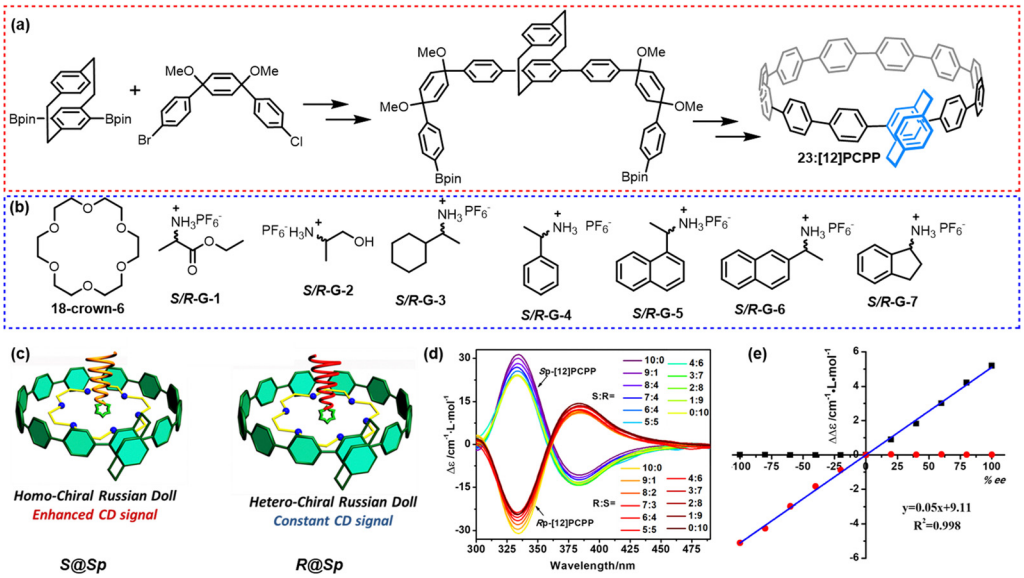

Fig. 12 The (a) synthetic procedure of 23, (b) the structure of the guests and (c–e) cartoon illustrations of self-assemblies of homochiral *S@Sp*- and heterochiral *R@Sp*-ternary complexes from **23** and their applications in narcissistic chiral self-recognitions. Adapted from ref. 47 with permission from Wiley-VCH, copyright 2024.

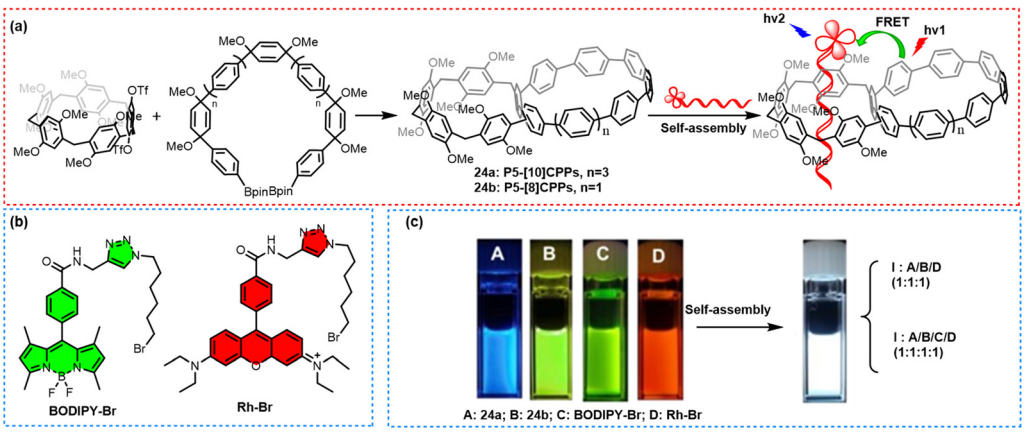

Fig. 13 (a, b) The construction of FRET systems based heterotopic bisnanohoops **24** and (c) their application on tunable white light emission. Adapted from ref. 48 with permission from the Royal Society of Chemistry, copyright 2023.

macrocycles for the development of hybrid supramolecular assemblies involving ring-in-ring complexes and smaller neutral guest molecules, while also highlighting the utility of FRET as a powerful tool for monitoring the formation of binary or Russian-doll complexes.

The integration of supramolecular engineering into the design of luminescent nanohoops offers a powerful strategy to manipulate photophysical properties through non-covalent interactions and controlled self-assembly. CPP derivatives, with their intrinsic curvature and π-conjugated cavities, serve as ideal platforms for exploring supramolecular packing and optoelectronic behaviors. In 2025, our group[55] explored the acceptor engineering of quinone-based CPPs to achieve white-light emission in single-molecules. By employing a post-synthetic strategy involving Diels–Alder reactions with **25a** (oxTh[10]CPP), a series of [10]CPPs **25b–25d** (Nq[10]CPP, Aq[10]-CPP, and Tq[10]CPP) were efficiently synthesized (Fig. 15). X-ray crystallographic analysis revealed that the structural differences of the CPPs led to unique packing arrangements, with **25b** showing side-by-side naphthoquinone stacking and **25c** adopting an intercalated conformation. Notably, fluorescence studies and theoretical calculations indicated that the quinone-based [10]CPPs exhibited acceptor-dependent dual emissions from both locally excited (LE) and charge-transfer (CT) states upon single-wavelength excitation. In particular, **25c** achieved white-light emission in $CHCl_3$, with CIE coordinates of (0.33, 0.25). The research also demonstrated the tunability of dual-emission properties through solvent polarity, aggregation, and redox reactions. In a THF/water mixture, the quinone-based [10]CPPs and **25a** exhibited a broad range of fluorescence emissions,

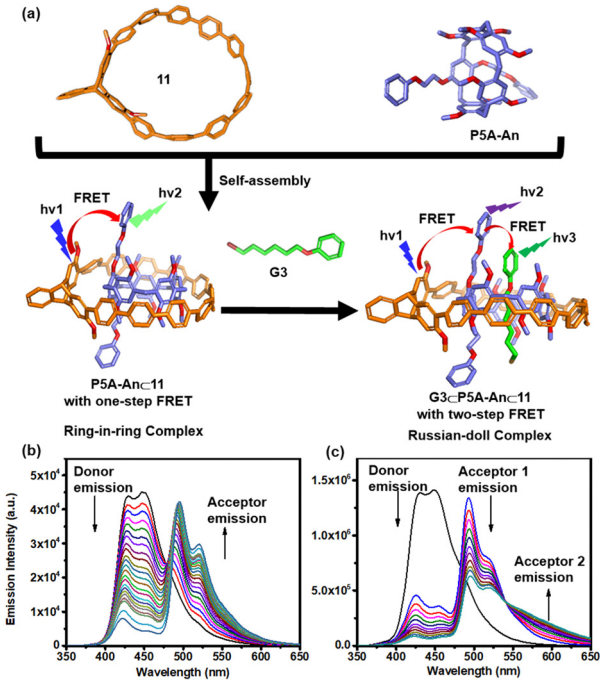

Fig. 14 (a) The construction of FRET systems-based compound **11**. Fluorescence emission spectra of the (b) ring-in-ring complexes and (c) the Russian-doll complexes. Adapted from ref. 54 with permission from American Chemical Society, copyright 2024.

including white-light, as the water fraction increased, accompanied by nanoparticle formation evidenced by the Tyndall effect and SEM. Interestingly, the fluorescence of **25c** could be switched from white to blue in $CHCl_3$ upon redox manipulation.

In 2024, a notable advancement in the construction of conjugated nanobelts was achieved through both symmetrical and asymmetrical longitudinal π-extensions of [12]CPP, as reported by Tan and coworkers.[56] Three distinct nanobelts, designated as **26a–26c** (Fig. 16), were synthesized, and their structures were unequivocally confirmed using single-crystal X-ray diffraction analysis. The incorporation of fused aromatic units into these nanobelts resulted in effective electronic conjugation, which was evidenced by red-shifted emission spectra. The design of these nanobelts leveraged the matched size and π–π interactions of the fused aromatic units, facilitating the stable double-walled assembly of **26b** and **26c**. Specifically, [9]CPP within **26b** was found to insert into [15]CPP of **26c**, forming a unique double-walled complex, **26b**⊃**26c**. Upon photoexcitation, this complex exhibited emission solely from **26b**, indicating complete intermolecular energy transfer from **26c** to **26b**. This phenomenon underscores the potential of such structures in studying energy transfer mechanisms. The efficient energy transfer observed in the double-walled **26b**⊃**26c** complex provides a valuable molecular model for understanding intertube energy transfer in multiwalled carbon nanotubes (CNTs).

Very recently, Itami[57] successfully synthesized **29** (PF[12]CPP⊃(6,6)CNB), the shortest fragment of double-walled noncovalent CNTs reported to date (Fig. 17). Time-dependent ^{1}H NMR and thermogravimetric analysis revealed that the encapsulation of **28** ((6,6)CNB) within **27** (PF[12]CPP) significantly enhanced its stability, highlighting the protective role of the host framework. The structural organization of **27** and **28** was found to be highly dependent on the crystallization conditions. When crystallized from chloroform/pentane, the complex adopted a "dimeric" brickwall alignment, whereas crystallization from 1,1,1-trichloroethane/octane resulted in a brickwall packing arrangement. Interestingly, crystallization from chloroform alone led to a tubular arrangement, demonstrating that the encapsulated solvent molecules play a critical role in dictating the packing structure. This solvent-directed assembly underscores the dynamic nature of the system and its responsiveness to environmental conditions. The tubular arrangement observed in this study represents a novel class of double-walled noncovalent CNTs. These structures are expected to exhibit high structural uniformity and resilience, making them promising candidates for advanced supramolecular materials. Furthermore, they serve as a molecularly defined model system for understanding and constructing double-walled CNTs with precise control over their architecture and properties.

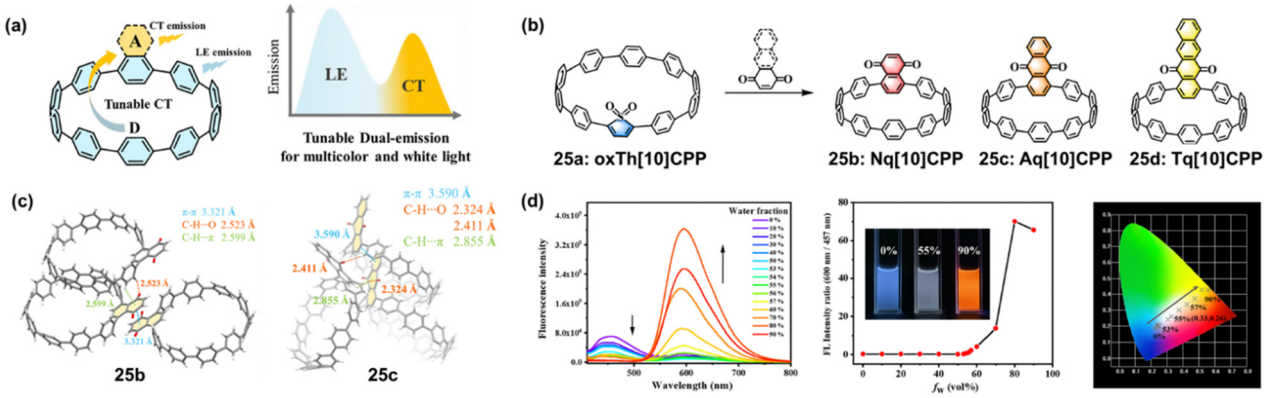

Fig. 15 (a) Conceptional strategy for constructing nanohoops with dual-emission states. (b) The structure of nanohoops **25a–25d**. (c) X-ray crystal structures of **25b** and **25c**. (d) Changes of fluorescence emission spectra and fluorescence colors of compound **25c** with different water fractions in THF solvent. Adapted from ref. 55 with permission from Springer Nature, copyright 2025.

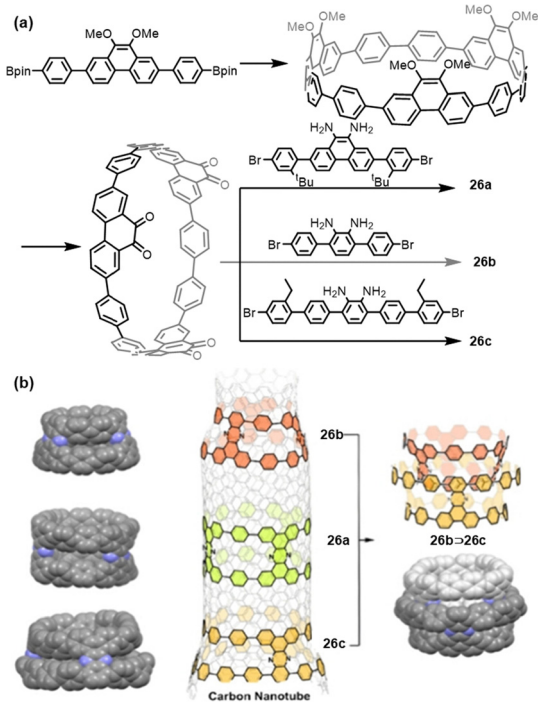

Fig. 16 The (a) synthetic procedures and (b) construction of FRET system-based compound **26**. Adapted from ref. 56 with permission from American Chemical Society, copyright 2025.

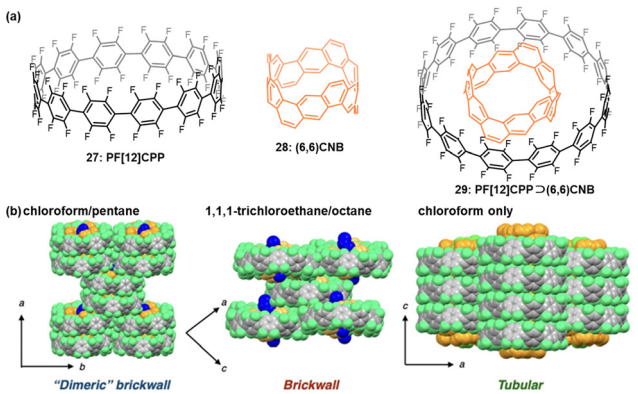

Fig. 17 (a) The chemical structure of **27–29**. (b) ORTEP and packing structures of PF[12]CPP⊃(6,6)CNB. Adapted from ref. 57 with permission from Wiley-VCH, copyright 2024.

The chemistry of CPP mechanically interlocked molecules is expected to facilitate the development of physical properties beyond the exciting topology. In 2018, Cong[58] and coworkers reported an efficient and precise synthesis of catenane **30** consisting of two mechanically linked, fully conjugated nanohoops *via* Sauvage's copper(I)-templated method (Fig. 18). Its crystal structure exhibits unusual topology, representing a rare case of a stabilized Möbius twisted π-system in the solid state. Theoretical calculations reveal the aromaticity in the monomer nanohoop as well as a strong driving force for the stabilization of catenane **30** through non-covalent π–π interaction. In 2019,

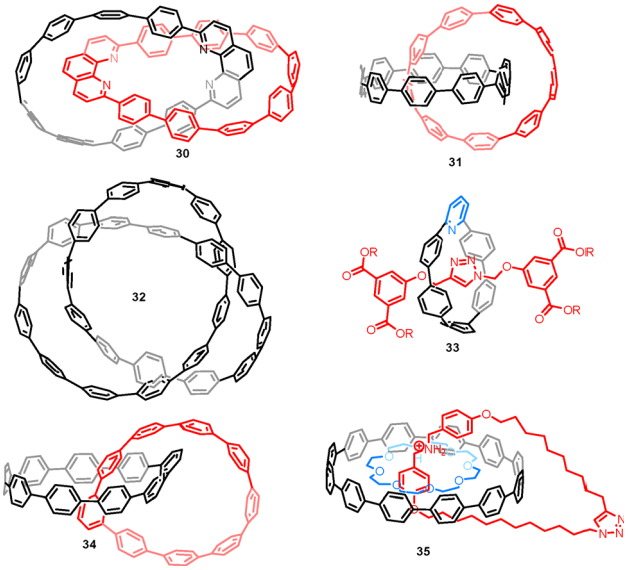

Fig. 18 Structures of CPP MIM **30–35**.

Itami *et al.*[59] successfully developed a novel traceless covalent template approach to achieve the synthesis of catenanes **31** and a molecular trefoil knot **32** composed exclusively of *para*-connected benzene rings. The interlocked structures were confirmed *via* X-ray crystallography. Characteristic fluorescence associated with rapid energy transfer between the two rings was observed in a heterocatenane system. Additionally, the topological chirality of the all-benzene knot **32** was validated through enantiomer separation and circular dichroism spectroscopy. Despite its apparent rigidity, the all-benzene knot exhibits rapid vortex-like motion in solution, even at −95 °C, leading to averaged nuclear magnetic resonance signals for all hydrogen atoms.

Subsequently, Jasti[60] reported the incorporation of a 2,6-pyridine coordination motif into the backbone of a nanohoop macrocycle. This design enables the synthesis of a diverse range of [2]rotaxanes **33** with high emissivity through two distinct CuI-catalyzed active-metal template reactions. Furthermore, the metal coordination, an intrinsic property conferred by the resulting mechanical bond, facilitates molecular shuttling and modulates fluorescence under both organic and aqueous conditions. Inspired by these findings, a self-immolative [2]rotaxane was designed to undergo self-destruction in the presence of an analyte, thereby eliciting a strong fluorescent turn-on response. This serves as a proof-of-concept for a novel class of molecular sensing materials. In 2022, Cong[61] developed a conjugated covalent template strategy based on the azo group and successfully applied this approach to synthesize a novel all-benzene catenane **34**. A key feature of this innovative synthetic strategy is the use of a tetra-substituted azobenzene core as a rigid π-conjugated synthon, which facilitates dual intramolecular macrocyclizations with high efficiency. Furthermore, the resulting precatenane can be effectively converted into the target catenane *via* a two-step process involving the traceless removal of the azo linker.

Notably, in addition to these remarkable synthetic studies, Cong,[62] Jasti,[63] Delius[64] and Itami[65] also achieved the elegant synthesis of analogous [2]catenanes and rotaxanes based on topologically complex nanocarbons.

Recently, Xu[66] and coworkers successfully synthesized a rare ABC-type hetero-[3]catenane **35** using an innovative ring-in-ring assembly strategy, incorporating unmodified [12]CPP, 24-crown-8, and a dibenzylammonium macrocycle. The structural and assembly properties of the binary [12]CPP⊂24-crown-8 and ternary [12]CPP⊂24-crown-8⊂dibenzylammonium complexes were elucidated through X-ray crystallography, providing critical insights into the pre-organization and mechanical bonding of the system. Photophysical characterization revealed that the introduction of flexible macrocycles had only a modest impact on the absorption and fluorescence properties of [12]CPP, preserving its intrinsic optical behavior. Molecular dynamics simulations provided detailed insights into the internal dynamics of the catenane, demonstrating that the larger [12]CPP ring can undergo slippage across the smaller 24-crown-8 ring. These simulations also highlighted the critical role of the protonation state of the dibenzylammonium moiety in modulating the dynamics of the system, suggesting a potential avenue for controlling the catenane's behavior through pH changes.

4. CPP derivatives and their applications in organic optoelectronic materials

4.1 [*n*]CPPs

CPPs, characterized by their rigid and cyclic π-electron systems, represent an exceptional structural platform for advanced organic optoelectronic materials. A particularly intriguing aspect of CPPs lies in their tunable optoelectronic properties, which can be precisely modulated through ring size variation. For instance, Zhu[67] *et al.* demonstrated that [*n*]CPPs (*n* = 5 to 12) exhibit higher conductance than linear oligoparaphenylenes at smaller ring sizes, due to their radially π-conjugated structures. Notably, the HOMO–LUMO gap of CPPs decreases as the molecular size reduces, contrasting with linearly conjugated molecules. This unique feature enables CPPs to achieve enhanced conductance at shorter lengths, making them highly suitable for nanoscale electronic applications. Moreover, CPPs exhibit excellent solubility and film-forming capabilities, complemented by their ability to self-assemble into ordered structures. These properties not only simplify device fabrication but also facilitate the development of molecular devices with tunable transport properties, further underscoring their potential in organic optoelectronics.

CPPs can serve as promising organic luminophores for transparent luminescent solar concentrators (LSCs). Traditional LSCs often suffer from reabsorption losses, where emitted light is reabsorbed by the fluorophores, reducing overall efficiency. However, CPPs, particularly [8]CPP and [10]CPP, exhibit remarkably large Stokes shifts of 1.4 eV and 1.07 eV,

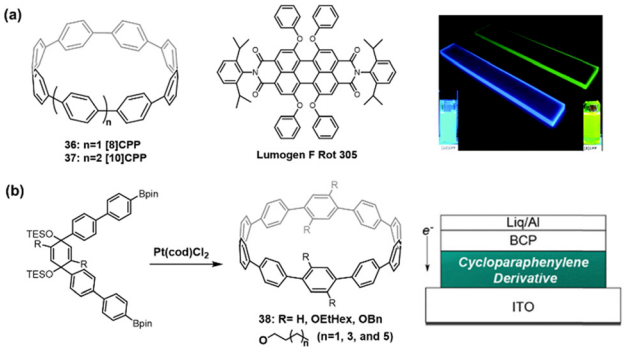

Fig. 19 (a) $CHCl_3$ solutions and PMMA slabs containing [8]CPP **33** and [10]CPP **34** under UV light irradiation at λ = 365 nm. Adapted from ref. 68 with permission from the Royal Society of Chemistry, copyright 2019. (b) CPP derivatives **38** as an electron-transport material in electron-only devices. Adapted from ref. 69 with permission from the American Chemical Society, copyright 2017.

respectively, which significantly reduce reabsorption losses.[68] In 2019, Gaeta[67] and colleagues successfully embedded these CPP derivatives into poly(methyl methacrylate) (PMMA) slabs using a photopolymerization method, preserving their spectral properties and enhancing their luminescence quantum yields. Notably, the luminescence efficiency of [8]CPP **36** increased from 10% in solution to 14% in PMMA, while that of [10]CPP **37** improved from 65% to 78% (Fig. 19a). The resulting LSCs demonstrated minimal reabsorption and scattering losses, with only about 10% attenuation of guided luminescence over optical distances as long as 18 cm, compared to 40% attenuation in traditional Lumogen R 305-based LSCs at just 3 cm, indicating that CPPs are highly suitable for developing transparent LSCs with potential applications in building-integrated photovoltaics.

Furthermore, CPP and their derivatives also have potential for constructing electron-transport materials. In 2017, Yamago *et al.*[69] reported the gram-scale synthesis and conductivity investigation of [10]CPP and its tetraalkoxy derivatives **38** (Fig. 19b). The researchers achieved the synthesis of **38** in just 7 steps, starting from 1,4-benzoquinone or 2,5-dialkoxy-1,4-benzoquinone, with an overall yield of 17% for [10]CPP. This represents a significant improvement over previous methods that required 10 steps and yielded only 7%. Moreover, thin films of CPPs were measured for their carrier transport properties, revealing that these materials could rival phenyl-C_{61}-butyric acid methyl ester (PCBM), a widely used n-type active layer in bulk heterojunction photovoltaics. Specifically, the ionization potential and electron affinity of **38** were found to be around 6.0 eV and 3.3 eV, respectively, comparable to those of PCBM (IP = 6.1 eV, EA = 3.9 eV). Additionally, the electron mobility was measured to be 4.5×10^{-6} cm^2 V^{-1} s^{-1} at 0.7 MV cm^{-1}, setting a valuable benchmark for further developing [10]CPP derivatives with enhanced electronic properties for organic electronics applications.

In 2019, the Du group[70] successfully synthesized a novel π-extended polymer **39** (PS1) containing a bifunctionalized CPP monomer into a poly(*para*-phenylene) backbone, representing

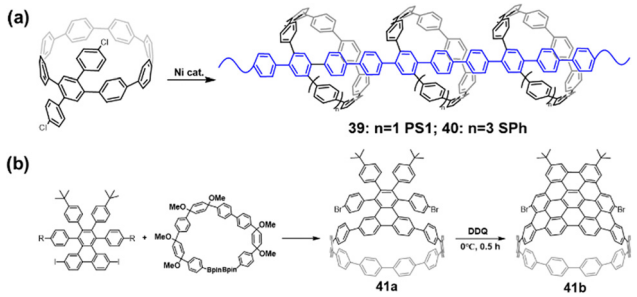

Fig. 20 (a) The synthetic procedure of CPP-based polymers **39–40** and (b) nanographene-embedded CPP **41b**.

the first polymeric segment of armchair [8,8] single-walled carbon nanotubes (SWCNTs) (Fig. 20a). The charge carrier mobilities of **39** in both electron and hole transport layers were measured using the space charge limited current (SCLC) method. In the electron-only device (ITO/ZnO/PS1/Ca/Al), the electron mobility of **39** was found to be approximately 2.0×10^{-5} cm^2 V^{-1} s^{-1}, while in the hole-only device (ITO/PSS/PS1/MoO_3/Ag), the hole mobility was measured to be around 1.2×10^{-5} cm^2 V^{-1} s^{-1}. These results demonstrate that **39** exhibits promising charge transport properties for both electron and hole transport layers, highlighting its potential applications in optoelectronic devices. Furthermore, wide-angle X-ray diffraction (WAXD) analysis revealed that it possesses a certain degree of crystallinity, further supporting its suitability for device applications.

Building on this, in 2021, this group[71] further expanded the applications of CPP-based polymers by designing and synthesizing a novel all-carbon supramolecular polymer host **40** (SPh), which forms a supramolecular polymeric heterojunction **40**⊃C_{60}. Femtosecond transient absorption and fluorescence up-conversion measurements revealed that photoexcited **40** transfers electrons to C_{60} within less than 300 femtoseconds, followed by charge recombination in the nanosecond timescale to produce the triplet excited state of C_{60}. In device testing, the electron mobility of **40**⊃C_{60} was found to be 8.06×10^{-5} cm^2 V^{-1} s^{-1}, while the hole mobility was significantly enhanced to 3.64×10^{-4} cm^2 V^{-1} s^{-1}. These results indicate that the incorporation of C_{60} markedly improves the charge transport properties of **40**, thereby validating the potential application of CPP-based polymers in optoelectronic devices.

In 2021, Du[72] and colleagues reported the synthesis of a nanographene-embedded CPP **41b** *via* the Scholl reaction, demonstrating its promising potential as an electron-transport material (Fig. 20b). Compared to its precursor **41a**, compound **41b** exhibited significant redshifts in both absorption and emission spectra, attributed to enhanced π-conjugation, which increased molecular rigidity and reduced the HOMO–LUMO gap from 3.17 eV in **41a** to 2.79 eV in **41b**. The electron mobility of **41b**, measured using the SCLC method, reached approximately 1.8×10^{-4} cm^2 V^{-1} s^{-1}, surpassing that of precursor 9 (1.4×10^{-4} cm^2 V^{-1} s^{-1}) and exceeding the electron mobility of other nanoring derivatives by a factor of **40**. This enhancement in electron transport properties is attributed to the extended π-conjugation and the curved crown-shaped structure of **41b**. The device performance was evaluated using electron-only devices with the structure ITO/ZnO/10/Ca/Al, highlighting the potential of CPP derivatives as an efficient electron-transport layer in organic electronic devices.

4.2 Donor–acceptor CPPs

The incorporation of electron donor (D) and acceptor (A) units into the framework of [*n*]CPPs has also emerged as a promising strategy for precisely modulating their electronic structures and expanding their potential applications in advanced technologies, including organic light-emitting diodes (OLEDs),[73] organic semiconductors (OSCs),[74] and biological imaging.[75] Currently, the synthesis of D–A integrated nanohoops is primarily achieved through two distinct strategies: selective incorporation of individual donor or acceptor moieties, or simultaneous integration of non-benzene donors and acceptors. These approaches have yielded diverse D–A CPP architectures, such as those incorporating pyridinium,[76,77] carbonyl,[78] fluorenone,[79] 2-(9*H*-fluoren-9-ylidene)malononitrile[79] and benzothiadiazole[80,81] as acceptors into the CPP skeleton; or introducing dimethoxynaphthalene as a donor paired with phthalate or phthalimide as acceptors;[82] bithiophene as a donor with a perylene diimide derivative as an acceptor;[83] and thiophene as a donor with 9-fluorenone as an acceptor,[84] among others.

Through systematic variation of the chemical properties and spatial arrangement of these D–A units, researchers can precisely control the HOMO–LUMO energy gap and charge transfer mechanisms, which are crucial for optimizing material performance in device applications. In 2015, Itami[85] and co-workers reported the first D–A CPP. Specifically, the introduction of anthraquinone (AQ, [10]CPAq) and tetracyanoanthraquinodimethane (TCAQ, [10]CPTcaq) as acceptors significantly lowered the LUMO energies to −2.71 eV and −3.55 eV, respectively, compared to −1.64 eV in the [12]CPP. This led to smaller HOMO–LUMO gaps and pronounced solvatofluorochromic behavior, exemplified by the fluorescence of [10]CPAq shifting from green to orange as solvent polarity increased.

The introduction of certain electron donors has facilitated the application of CPPs in the field of organic electronic devices. In 2022, Quinton[86] and co-workers reported a series of donor carbazole-bridged CPPs with varying ring sizes, **42a–42c** ([16]CPP4N, [12]CPP3N, and [8]CPP4N) (Fig. 21a). The study demonstrated that modulating the number of donor carbazole and acceptor phenylene units enables precise tuning of the HOMO/LUMO energy levels. Specifically, the removal of a carbazole-based building unit predominantly enhanced the reduction capability, while the elimination of all phenylenes significantly improved the oxidation capability. Moreover, the removal of all phenylenes effectively reduced intermolecular interactions in the solid state, and increasing the number of donor units enhanced dipole–dipole interactions between the nanohoops and polar solvent molecules, leading to greater stabilization of the excited state. These findings establish a robust framework for designing nanohoop-based OSCs to suit specific application demands.

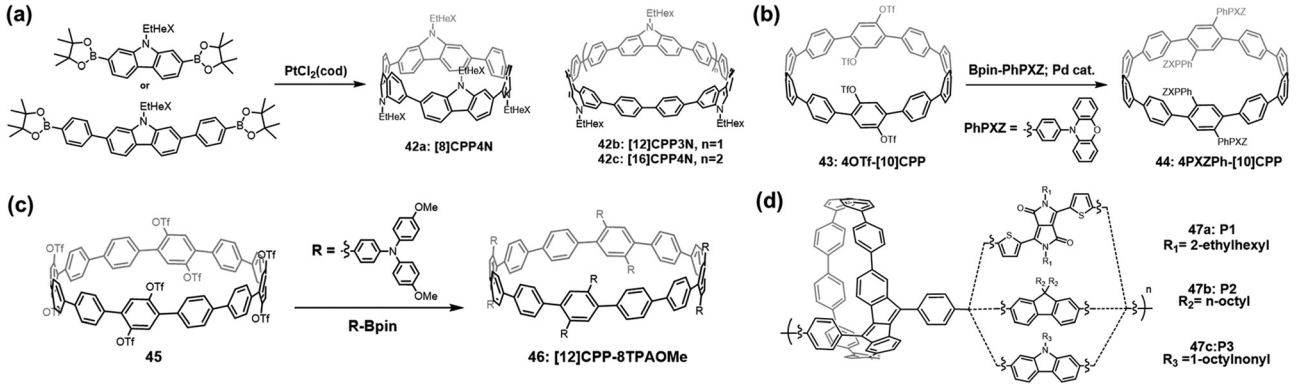

Fig. 21 Structures of (a) carbazole-bridged CPPs **42a–42c**, D–A CPPs incorporating (b) phenoxazine **44** and (c) di(4-methoxyphenyl)amino **46** moieties, and (d) CPP-based copolymers with dibenzo[a,e]pentalene as a central connector **47a–47c**.

In 2023, Yamago[72] and colleagues designed a CPP derivative, **44** (4PXZPh-[10]CPP), by incorporating four phenoxazine as electron donors, with the aim of achieving thermally activated delayed fluorescence (TADF) (Fig. 21b). Density functional theory calculations demonstrated that **44** exhibits a favorable spatial separation between the HOMO and LUMO, accompanied by a small predicted singlet–triplet energy gap (ΔE_{ST}) of 0.08 eV. The synthesized compound displayed green emission in toluene (λ_{PL} = 508 nm) with a photoluminescence quantum yield (Φ_{PL}) of 34% and a prompt lifetime of 11.0 ns. When doped into the ambipolar host CzSi at 15 wt%, **44** exhibited moderately bright sky-blue emission (λ_{PL} = 475 nm) with a Φ_{PL} of 29%. Solution-processed OLEDs utilizing **44** as the emitter achieved sky-blue electroluminescence (λ_{EL} = 465 nm) with a maximum external quantum efficiency (EQE_{MAX}) of 1.0%. However, the device performance was constrained by a combination of low Φ_{PL} and inefficient reverse intersystem crossing.

In 2024, Du[87] and colleagues reported the synthesis, photophysical properties, and charge transport characteristics of a novel intramolecular D–A system, **46** ([12]CPP-8TPAOMe), functionalized with eight di(4-methoxyphenyl)amino groups as electron donors (Fig. 21c). Compared to [12]CPP (446 nm), **46** shows a significant redshift in emission to 524 nm, along with remarkable solvatofluorochromism, transitioning from blue in toluene (484 nm) to yellow in DMF (546 nm). Furthermore, **46** demonstrates distinctive bipolar charge transport behavior, with both electron and hole mobilities reaching the order of 10^{-5} cm^2 V^{-1} s^{-1} when utilized as the active layer in organic field-effect transistors (OFETs).

In 2023, the Esser group[88] reported a versatile synthetic approach for conjugated nanohoop polymers, employing dibenzo[*a*,*e*]pentalene (DBP) as a central connector. Three distinct copolymers **47a-42c** (P1, P2 and P3) were synthesized by incorporating electronically diverse comonomers: dithienyldiketo-(pyrrolopyrrole) (DTDPP, electron-deficient), fluorene (electronically neutral), and carbazole (electron-rich) (Fig. 21d). The DTDPP-based copolymer **47a** exhibited D–A characteristics, with a strong absorption band centered at 592 nm and a dual emission profile at 644 nm and 473 nm, indicating dominant linear conjugation along the polymer backbone. In contrast, the fluorene **47b** and carbazole **47c** copolymers showed cyclic conjugation within the nanohoops, with absorption maxima around 342–345 nm and emission maxima at 470 nm, closely resembling the reference DBP nanohoop. The antiaromatic character of DBP imparts ambipolar electrochemical properties to these polymers, endowing them with broad application potential in organic batteries and electrochemical energy storage. Electrochemical studies revealed reversible redox activity for all polymers, with **47a** showing two reductions at approximately −1.58 V and three oxidations, the first at 0.40 V, while **47c** exhibited a significant oxidation current at 0.66 V, likely due to carbazole participation. When tested as positive electrode materials in lithium-organic half-cells, copolymer **47c** demonstrated superior performance, delivering a discharge capacity of 30 mA h g^{-1} in the first cycle and retaining 22.8 mA h g^{-1} after 100 cycles at 100 mA g^{-1}, with a capacity retention of 99%. In comparison, the nanohoop-free reference polymer achieved only 21.8 mA h g^{-1} initially, highlighting the enhanced charge storage capabilities of nanohoop polymers.

4.3 Supramolecular heterojunction based on CPPs

The unique concave–convex complementarity between the curved π-surface of CPPs and the spherical geometry of fullerenes facilitates the formation of stable host–guest complexes, primarily driven by π–π stacking and van der Waals interactions. These interactions not only stabilize the supramolecular assemblies but also induce charge transfer between CPPs and fullerenes, a phenomenon that has significant potential for the development of advanced optoelectronic devices.[12] In 2015, Itami[89] *et al.* synthesized the first CPP-based ionic donor–acceptor supramolecule $Li^+@C_{60}\subset$[10]CPP·X^-, highlighting the strong charge-transfer interaction between [10]CPP and $Li^+@C_{60}$. This interaction results in significant delocalization of the positive charge across the entire complex, with the positive charge of the lithium ion being distributed not only on the C_{60} cage but also on the outer CPP ring, as confirmed by electrochemical measurements and spectroscopic analyses. Further insights into the charge-transfer dynamics were provided by Casado[90] and colleagues, who revealed that mechanical stress can facilitate electron transfer between [*n*]CPPs and C_{60}. Under high pressure, [10]CPP and C_{60} form a

charge-transfer complex characterized by the generation of the C_{60} anion radical ($C_{60}^{\bullet-}$) and the [10]CPP cation radical ([10]CPP$^{\bullet+}$). Moreover, a study by the Delius[91] group in 2018 highlighted the potential of [10]CPP as a supramolecular mediator in facilitating efficient photoinduced electron transfer in modular porphyrin–[10]CPP–fullerene complexes. Synthetically, the construction of a porphyrin–[10]CPP conjugate *via* iodo-[10]CPP enabled the demonstration of strong binding affinities with fullerenes such as C_{60}, C_{70}, and $(C_{60})_2$, as well as their derivatives, with association constants (K_A) reaching 10^5–10^6 M^{-1}. The [10]CPP moiety served as a rigid, non-covalent bridge that enabled efficient photoinduced charge separation between the porphyrin donor and fullerene unit acceptors. Time-resolved transient absorption spectroscopy revealed the formation of long-lived charge-separated states, with lifetimes reaching up to 0.5 μs. These findings underscore the versatility of CPPs in modulating electron transfer processes and suggest its potential application in organic electronic devices.

In 2019, the Du[92] group reported the synthesis and characterization of two novel curved nanographene-based molecular crowns, **48** (TCR) and **49** (HCR), which exhibit strong supramolecular interactions with C_{60} (Fig. 22a). The binding constants for these complexes were determined to be 3.34×10^6 M^{-1} for **48**⊃C_{60} and 2.33×10^7 M^{-1} for **49**⊃C_{60}. Transient absorption spectroscopy revealed efficient photoinduced electron transfer from **48** and **49** to C_{60}, with charge-separated states exhibiting lifetimes in the nanosecond range. These complexes demonstrated significant photoconductive properties, generating stable photocurrents under visible light irradiation. Photocurrent measurements on FTO electrodes coated with C_{60}@**49** films exhibited a 1000-fold increase in current under irradiation, highlighting the potential of these supramolecular heterojunctions for light-to-electrical energy conversion materials.

In 2020, the Du[93] group also reported a novel strategy to enhance the performance of fullerene organic solar cells (OSCs) by incorporating [9]CPP as a third component in the active layer. The [9]CPP forms a stable supramolecular complex **50** with fullerene acceptors due to concave–convex π–π interactions, which improves the π–π stacking and enhances charge transfer and transport (Fig. 22b). This approach led to a significant increase in the short-circuit current density (J_{SC}) from 17.91 mA cm^{-2} to 19.27 mA cm^{-2} and the fill factor (FF) to 68%, resulting in a high power conversion efficiency (PCE) of 11.03% in PTB7-Th:[9]CPP:PC71BM ternary OSCs, which is nearly 20% higher than that of binary devices. The addition of [9]CPP also improved the absorption in the short-wave region (300–400 nm) and optimized the film morphology, forming a nano-inter-transmission network that further enhanced the device performance. This study demonstrates that [9]CPP can effectively improve the efficiency of fullerene-based OSCs by optimizing the molecular interactions and film structure.

In 2022, Zhang[94] *et al.* investigated the photoelectrochemical properties of three metallofullerene-[12]CPP supramolecular complexes, namely $Sc_3N@C_{78}$⊂[12]CPP, $Sc_3N@C_{80}$⊂[12]CPP, and

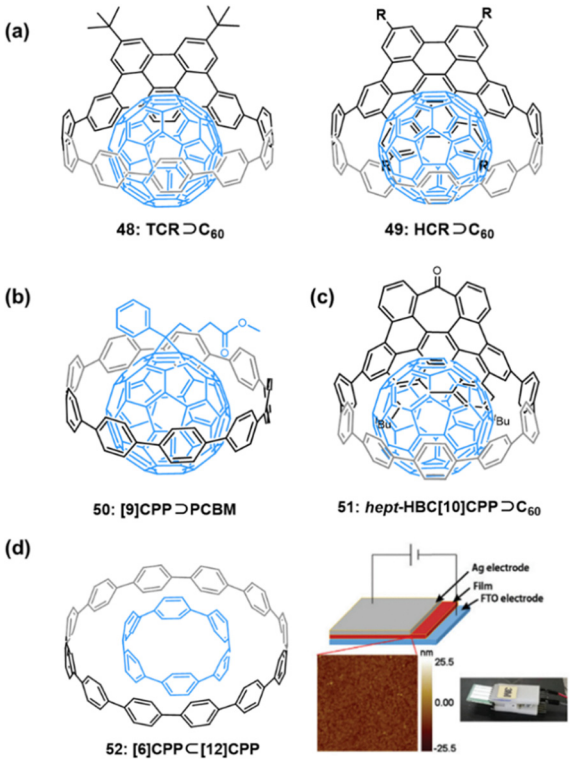

Fig. 22 Structures of (a) nanographene-based molecular crown complexes with C_{60} **48–49**, (b) [9]CPP complexes with PCBM **50**, (c) heptagon-containing CPP **51**, and (d) the double-walled carbon nanoring [6]CPP⊂[12]CPP **52** and the FTO/film/Ag device for photocurrent production. Adapted from ref. 97 with permission from the Royal Society of Chemistry, copyright 2021.

$Sc_2C_2@C_{82}$⊂[12]CPP, and explored their potential applications in photodetectors and photoelectronic materials. The study revealed that these supramolecular complexes demonstrated significantly enhanced photocurrent responses compared to their pristine metallofullerene counterparts. Notably, the photocurrent response of $Sc_2C_2@C_{82}$⊂[12]CPP reached 0.32 μA under a 1 V bias voltage, surpassing that of pristine $Sc_2C_2@C_{82}$ (0.2 μA). This enhancement is attributed to the efficient photocurrent generation and improved charge carrier transport facilitated by the host–guest interactions. Furthermore, the formation of supramolecular complexes also optimizes the assembly morphology of metallofullerenes on fluorine-doped tin oxide (FTO) glass, leading to increased carrier mobility and electrical conductivity. *I–V* measurements indicated that $Sc_2C_2@C_{82}$⊂[12]CPP exhibited superior conductivity compared to both pristine $Sc_2C_2@C_{82}$ and $Sc_2C_2@C_{82}$-biphenyl derivative mixtures. These findings underscore the potential of metallofullerene-CPP supramolecular complexes in advancing photoelectronic applications.

In 2023, a study by Campaña[95] and colleagues reported the efficient electron transfer between a heptagon-containing CPP **51** (*hept*-HBC[10]CPP) and fullerenes, driven by strong host–guest interactions (Fig. 22c). The binding constants for **51**⊃C_{60} and **51**⊃C_{70} were determined as 1.1×10^7 M^{-1} for C_{60} and 7.8×10^6 M^{-1} for C_{70}, respectively. Femtosecond transient

absorption spectroscopy revealed ultrafast charge separation upon photoexcitation. While **51**⊃C_{60} exhibited rapid charge recombination (τ_1 = 110 fs, τ_2 = 800 fs), the **51**⊃C_{70} complex displayed a long-lived charge-separated state, persisting beyond the picosecond timescale. This difference indicates that the choice of fullerene guest can modulate the electron-transfer dynamics, enabling the system to adapt to applications requiring controlled charge separation, with implications for advanced material design in photovoltaics and photocatalysis.

In 2025, our group[96] synthesized a series of nanohoops, NDI-[*n*]CPP (*n* = 7, 8, 9), by incorporating naphthalene diimide (NDI) as an electron acceptor into CPP frameworks (Fig. 23). These nanohoops exhibit size-dependent photophysical properties, with fluorescence emission shifting from 599 nm for **53a** (NDI-[7]CPP) to 578 nm for **53c** (NDI-[9]CPP). Their HOMO–LUMO gaps range from 2.38 eV for **53c** to 2.42 eV for **53a**, significantly narrower than those of the parent [*n*]CPPs. In photoconductive applications, NDI-[*n*]CPPs generate significant photocurrents under visible light, with **53a** showing the highest photocurrent density of 10.17 μA cm^{-2}. Notably, the photocurrent of **53a** is enhanced by 3.46 times upon complexation with C_{60}. These nanohoops also demonstrate moderate electron and hole mobilities, with **53a** showing balanced hole mobility (μ_h)/electron mobility (μ_e) ratios suitable for efficient charge collection.

Apart from fullerenes and their derivatives, CPP itself can also serve as a guest molecule to be included in larger nanohoops. In 2021, Zhao[97] *et al.* reported the construction of a double-walled carbon nanoring [6]CPP⊂[12]CPP **52**, which can be considered as the fragment of a double-walled carbon nanotube (Fig. 22d). The host–guest interaction between [6]CPP and [12]CPP was thoroughly investigated through UV-Vis absorption, fluorescence, and electrochemical studies. The HOMO–LUMO gap of [6]CPP⊂[12]CPP (2.9 eV) was narrowed compared to the individual CPPs. Electron paramagnetic resonance (EPR) spectroscopy revealed that the cation radical of [6]CPP⊂[12]CPP had higher stability due to the host–guest interaction, with the unpaired spin fully delocalized on the inner [6]CPP and protected by the outer [12]CPP. Moreover, the complex showed significantly enhanced photoconductivity and photocurrent under light irradiation, with the current increasing by about twice upon uninterrupted irradiation. The impedance of [6]CPP⊂[12]CPP decreased from 4.65 × 10^6 to 4.24 × 10^5 Ω cm^2 after irradiation, indicating improved conductivity. The self-assembly of [6]CPP⊂[12]CPP in DMF forms square rod structures, highlighting its potential for micro-device applications.

5. Summary and outlook

CPPs, characterized by intrinsic curvature, tunable electronic configurations, and size-dependent π-conjugation, have evolved into a multifunctional molecular platform. Over the past years, our group has focused on innovative methodologies to expand the structural and functional diversity of CPP-based systems. Through strategic incorporation of chiral or achiral motifs into CPP frameworks, we engineered high-brightness CPL emitters, advancing chiral photonic technologies. Within the field of host–guest chemistry, stimuli-responsive CPP derivatives capable of dynamically modulating guest-binding affinities have been engineered. Moreover, the formation of binary and ternary complexes through precisely tailored CPP hosts has been demonstrated, facilitating Förster resonance energy transfer and selective molecular recognition. In the topological chemistry, systematic exploration of regioselective synthesis strategies has provided insights into the control of topological chirality. Concurrently, the development of donor–acceptor CPPs has demonstrated their potential in white-light emission tuning and integration into optoelectronic devices. These advancements collectively demonstrate the unparalleled potential of CPPs in constructing topologically sophisticated

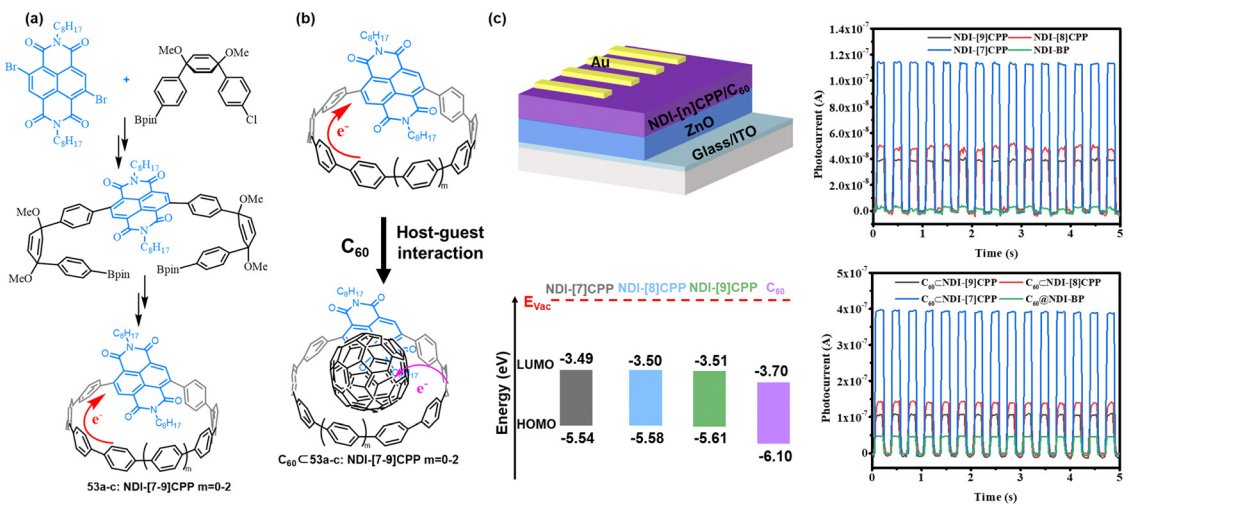

Fig. 23 Structures of (a) NDI-[*n*]CPP **53a–53c** and (b) their complexes with C_{60}, and (c) device for photocurrent production. Adapted from ref. 96 with permission from American Chemical Society, copyright 2025.

systems with functionalities for next-generation materials science. Despite these advancements, several challenges and opportunities remain to propel CPP chemistry toward practical applications and unexplored frontiers. As synthetic methodologies mature and structure–property relationships deepen, CPP-based systems are poised to revolutionize fields ranging from nanotechnology to sustainable energy.

Data availability

No primary research results, software or code have been included and no new data were generated or analysed as part of this review.

Conflicts of interest

There are no conflicts to declare.

Acknowledgements

This work was financially supported by the National Natural Science Foundation of China (22271019 and 22471022).

Notes and references

1 F. Diederich, Y. Rubin, C. B. Knobler, R. L. Whetten, K. E. Schriver, K. N. Houk and Y. Li, *Science*, 1989, **245**, 1088–1090.
2 J. F. Stoddart, *Nature*, 1989, **342**, 482–483.
3 J. F. Stoddart, *Angew. Chem., Int. Ed. Engl.*, 1991, **30**, 70–71.
4 J. S. Siegel, *Science*, 2017, **356**, 135–136.
5 H. W. Kroto, J. R. Heath, S. C. O'Brien, R. F. Curl and R. E. Smalley, *Nature*, 1985, **318**, 162–163.
6 R. E. Smalley, *Angew. Chem., Int. Ed. Engl.*, 1997, **36**, 1594–1601.
7 H. Kroto, *Angew. Chem., Int. Ed. Engl.*, 1997, **36**, 1578–1593.
8 R. F. Curl, *Angew. Chem., Int. Ed. Engl.*, 1997, **36**, 1566–1576.
9 S. Iijima, *Nature*, 1991, **354**, 56–58.
10 R. Jasti, J. Bhattacharjee, J. B. Neaton and C. R. Bertozzi, *J. Am. Chem. Soc.*, 2008, **130**, 17646–17647.
11 G. Povie, Y. Segawa, T. Nishihara, Y. Miyauchi and K. Itami, *Science*, 2017, **356**, 172–175.
12 E. J. Leonhardt and R. Jasti, *Nat. Rev. Chem.*, 2019, **3**, 672–686.
13 Y. M. Li, H. Kono, T. Maekawa, Y. Segawa, A. Yagi and K. Itami, *Acc. Mater. Res.*, 2021, **2**, 681–691.
14 T. J. Sisto, M. R. Golder, E. S. Hirst and R. Jasti, *J. Am. Chem. Soc.*, 2011, **133**, 15800–15802.
15 M. Hermann, D. Wassy and B. Esser, *Angew. Chem., Int. Ed.*, 2021, **60**, 15743–15766.
16 S. Yamago, Y. Watanabe and T. Iwamoto, *Angew. Chem., Int. Ed.*, 2010, **49**, 757–759.
17 H. Takaba, H. Omachi, Y. Yamamoto, J. Bouffard and K. Itami, *Angew. Chem., Int. Ed.*, 2009, **48**, 6112–6116.
18 Y. Tsuchido, R. Abe, T. Ide and K. Osakada, *Angew. Chem., Int. Ed.*, 2020, **59**, 22928–22932.
19 D. Zheng, L. Zheng, C. Y. Yu, Y. L. Zhan, Y. Wang and H. Jiang, *Org. Lett.*, 2019, **21**, 2555–2559.
20 C. B. Du, Y. J. Long, X. N. Han, Y. Han and C. F. Chen, *Chem. Commun.*, 2024, **60**, 13492.
21 L. Zheng, Y. Zhan, L. Ye, D. Zheng, Y. Wang, K. Zhang and H. Jiang, *Chem. – Eur. J.*, 2019, **25**, 14162–14168.
22 D. Zheng, C. Y. Yu, L. Zheng, Y. L. Zhan and H. Jiang, *Chin. Chem. Lett.*, 2020, **31**, 673.
23 H. Omachi, Y. Segawa and K. Itami, *Org. Lett.*, 2011, **13**, 2480–2483.
24 J. Wang, H. Shi, S. Wang, X. Zhang, P. Fang, Y. Zhou, G. L. Zhuang, X. Shao and P. Du, *Chem. – Eur. J.*, 2022, **28**, e202103828.
25 A. Li, X. Zhang, S. Wang, K. Wei and P. Du, *Org. Lett.*, 2023, **25**, 1183–1187.
26 X. Kong, X. Zhang, B. Yuan, W. Zhang, D. Lu and P. Du, *J. Org. Chem.*, 2024, **89**, 8255–8261.
27 K. Sato, M. Hasegawa, Y. Nojima, N. Hara, T. Nishiuchi, Y. Imai and Y. Mazaki, *Chem. – Eur. J.*, 2021, **27**, 1323–1329.
28 P. Fang, M. Chen, X. Zhang and P. Du, *Chem. Commun.*, 2022, **58**, 8278–8281.
29 Q. Huang, J. Zhang, H. Chen, X. Kong, P. Xu and P. Du, *Org. Chem. Front.*, 2023, **10**, 911–915.
30 L. H. Wang, N. Hayase, H. Sugiyama, J. Nogami, H. Uekusa and K. Tanaka, *Angew. Chem., Int. Ed.*, 2020, **59**, 17951–17957.
31 J. He, M. Yu, M. Pang, Y. Q. Fan, Z. Lian, Y. Wang, W. G. Wang, Y. Liu and H. Jiang, *Chem. – Eur. J.*, 2022, **28**, e202103832.
32 J. He, M. Yu, Z. Lian, Y. Q. Fan, S. Z. Guo, X. N. Li, Y. Wang, W. G. Wang, Z. Y. Cheng and H. Jiang, *Chem. Sci.*, 2023, **14**, 4426–4433.
33 S. Z. Guo, L. Liu, X. N. Li, G. Q. Liu, Y. Q. Fan, J. He, Z. Lian, H. J. Yang, X. B. Chen and H. Jiang, *Small*, 2024, **20**, 2308429.
34 Y. Yoshigoe, H. Shimada, T. Takaki, Y. Imai and S. Saitolal, *Chem. – Eur. J.*, 2024, **30**, e202304059.
35 J. Malinčik, S. Gaikwad, J. P. Mora-Fuentes, M. A. Boillat, A. Prescimone, D. Häussinger, A. G. Campaña and T. Šolomek, *Angew. Chem., Int. Ed.*, 2022, **61**, e202208591.
36 H. J. Yang, S. Z. Guo, W. J. Guo, L. Liu, X. Y. Liu, J. He, Y. Q. Fan, Z. Lian, X. N. Li, S. Huang, X. B. Chen, Y. Wang and H. Jiang, *Chem. – Asian J.*, 2025, e00205.
37 K. Senthilkumar, M. Kondratowicz, T. Lis, P. J. Chmielewski, J. Cybińska, J. L. Zafra, J. Casado, T. Vives, J. Crassous, L. Favereau and M. Stępień, *J. Am. Chem. Soc.*, 2019, **141**, 7421–7427.
38 T. A. Schaub, E. A. Prantl, J. Kohn, M. Bursch, C. R. Marshall, E. J. Leonhardt, T. C. Lovell, L. N. Zakharov, C. K. Brozek, S. R. Waldvogel, S. Grimme and R. Jasti, *J. Am. Chem. Soc.*, 2020, **142**, 8763–8775.
39 Y. Zhang, D. Yang, S. H. Pun, H. Chen and Q. Miao, *Precis. Chem.*, 2023, **1**, 107–111.
40 W. Xu, X. D. Yang, X. B. Fan, X. Wang, C. H. Tung, L. Z. Wu and H. Cong, *Angew. Chem., Int. Ed.*, 2019, **58**, 3943–3947.
41 X. Zhang, H. Liu, G. Zhuang, S. Yang and P. Du, *Nat. Commun.*, 2022, **13**, 3543.
42 G. Li, L. L. Mao, J. N. Gao, X. Shi, Z. Y. Huo, J. Yang, W. Zhou, H. Li, H. B. Yang, C. H. Tung, L. Z. Wu and H. Cong, *Angew. Chem., Int. Ed.*, 2025, **64**, e202419435.
43 N. Liu, Y. Choi, Z. Zong, T. Feng, T. Kim and X. S. Ke, *CCS Chem.*, 2025, DOI: **10.31635/ccschem.025.202505435**.
44 W. Song, Z. Liu, X. Hua, S. Yang, X. Tang, C. Yuan, Z. Liu, H. L. Zhang and X. Shao, *Aggregate*, 2024, **5**, e646.
45 Y. Q. Fan, J. He, S. Z. Guo and H. Jiang, *ChemPlusChem*, 2024, **89**, e202300536.
46 X. N. Li, L. Jia, W. G. Wang, Y. Wang, D. Sun and H. Jiang, *J. Mater. Chem. C*, 2023, **11**, 1429.
47 Y. Q. Fan, J. He, L. Liu, G. Q. Liu, S. Z. Guo, Z. Lian, X. N. Li, W. J. Guo, X. B. Chen, Y. Wang and H. Jiang, *Angew. Chem., Int. Ed.*, 2023, **62**, e202304623.
48 Y. Q. Fan, S. M. Fan, L. Liu, S. Z. Guo, J. He, X. N. Li, Z. Lian, W. J. Guo, X. B. Chen, Y. Wang and H. Jiang, *Chem. Sci.*, 2023, **14**, 11121–11130.
49 Y. Q. Fan, *Doctoral dissertation of Beijing Normal University entitled "Synthesis and properties of carbon nanorings based on [2.2]PCP and pillar[5]arene units"*, 2023.
50 K. Kato, Y. Kurakake, S. Ohtani, S. Fa, M. Gon, K. Tanaka and T. Ogoshi, *Angew. Chem., Int. Ed.*, 2022, **61**, e202209222.
51 J. F. Chen, X. Yin, B. Wang, K. Zhang, G. Meng, S. Zhang, Y. Shi, N. Wang, S. Wang and P. Chen, *Angew. Chem., Int. Ed.*, 2020, **59**, 11267–11272.
52 H. Zhu, Q. Li, B. Shi, H. Xing, Y. Sun, S. Lu, L. Shangguan, X. Li, F. Huang and P. J. Stang, *J. Am. Chem. Soc.*, 2020, **142**, 17340–17345.
53 J. F. Chen, X. Yin, K. Zhang, Z. Zhao, S. Zhang, N. Zhang, N. Wang and P. Chen, *J. Org. Chem.*, 2021, **86**, 12654–12663.
54 S. Z. Guo, L. Liu, F. Su, H. J. Yang, G. Q. Liu, Y. Q. Fan, J. He, Z. Lian, X. N. Li, W. J. Guo, X. B. Chen and H. Jiang, *JACS Au*, 2024, **4**, 402–410.
55 X. N. Li, L. Liu, L. Y. Jia, Z. Lian, J. He, S. Z. Guo, Y. Wang, X. B. Chen and H. Jiang, *Nat. Commun.*, 2025, **16**, 467.

56 X. W. Chen, Q. S. Deng, B. H. Zheng, J. F. Xing, H. R. Pan, X. J. Zhao and Y. Z. Tan, *J. Am. Chem. Soc.*, 2024, **146**, 31665–31670.
57 D. Imoto, H. Shudo, A. Yagi and K. Itami, *Angew. Chem., Int. Ed.*, 2025, **64**, e202413828.
58 Y. Y. Fan, D. Chen, Z. A. Huang, J. Zhu, C. H. Tung, L. Z. Wu and H. Cong, *Nat. Commun.*, 2018, **9**, 3037.
59 Y. Segawa, M. Kuwayama, Y. Hijikata, M. Fushimi, T. Nishihara, J. Pirillo, J. Shirasaki, N. Kubota and K. Itami, *Science*, 2019, **365**, 272–276.
60 J. M. VanRaden, B. M. White, L. N. Zakharov and R. Jasti, *Angew. Chem., Int. Ed.*, 2019, **58**, 7341–7345.
61 A. Bu, Y. Zhao, H. Xiao, C. H. Tung, L. Z. Wu and H. Cong, *Angew. Chem., Int. Ed.*, 2022, **61**, e202209449.
62 A. Bu, J. N. Gao, Y. Chen, H. Xiao, H. Li, C. H. Tung, L. Z. Wu and H. Cong, *Angew. Chem., Int. Ed.*, 2024, **63**, e202401838.
63 C. W. Patrick, J. F. Woods, P. Gawel, C. E. Otteson, A. L. Thompson, T. D. W. Claridge, R. Jasti and H. L. Anderson, *Angew. Chem., Int. Ed.*, 2022, **61**, e202116897.
64 Y. Xu, R. Kaur, B. Wang, M. B. Minameyer, S. Gsänger, B. Meyer, T. Drewello, D. M. Guldi and M. von Delius, *J. Am. Chem. Soc.*, 2018, **140**, 13413–13420.
65 H. Ishibashi, M. Rondelli, H. Shudo, T. Maekawa, H. Ito, K. Mizukami, N. Kimizuka, A. Yagi and K. Itami, *Angew. Chem., Int. Ed.*, 2023, **62**, e202310613.
66 W. Shi, Y. Hu, L. Leanza, Y. Shchukin, P. A. Hoffmann, M. H. Li, C. Ning, Z. Y. Cao, Y. Q. Xu, P. Du, M. von Delius, G. M. Pavan and Y. Xu, *Angew. Chem., Int. Ed.*, 2025, **64**, e202421459.
67 Y. Lv, J. Lin, K. Song, X. Song, H. Zang, Y. Zang and D. Zhu, *Sci. Adv.*, 2021, **7**, eabk3095.
68 P. Della Sala, N. Buccheri, A. Sanzone, M. Sassi, P. Neri, C. Talotta, A. Rocco, V. Pinchetti, L. Beverina, S. Brovelli and C. Gaeta, *Chem. Commun.*, 2019, **55**, 3160–3163.
69 E. Kayahara, L. Sun, H. Onishi, K. Suzuki, T. Fukushima, A. Sawada, H. Kaji and S. Yamago, *J. Am. Chem. Soc.*, 2017, **139**, 18480–18483.
70 Q. Huang, G. Zhuang, M. Zhang, J. Wang, S. Wang, Y. Wu, S. Yang and P. Du, *J. Am. Chem. Soc.*, 2019, **141**, 18938–18943.
71 S. Wang, X. Li, X. Zhang, P. Huang, P. Fang, J. Wang, S. Yang, K. Wu and P. Du, *Chem. Sci.*, 2021, **12**, 10506–10513.
72 S. Wang, X. Li, G. Zhuang, M. Chen, P. Huang, S. Yang and P. Du, *Chem. Commun.*, 2021, **57**, 9104–9107.
73 D. Chen, Y. Wada, Y. Kusakabe, L. Sun, E. Kayahara, K. Suzuki, H. Tanaka, S. Yamago, H. Kaji and E. Zysman-Colman, *Org. Lett.*, 2023, **25**, 998–1002.
74 S. Canola, C. Graham, Á. J. Pérez-Jiménez, J.-C. Sancho-García and F. Negri, *Phys. Chem. Chem. Phys.*, 2019, **21**, 2057–2068.
75 K. Li, Z. Xu, H. Deng, Z. Zhou, Y. Dang and Z. Sun, *Angew. Chem., Int. Ed.*, 2021, **60**, 7649–7653.
76 E. R. Darzi, E. S. Hirst, C. D. Weber, L. N. Zakharov, M. C. Lonergan and R. Jasti, *ACS Cent. Sci.*, 2015, **1**, 335–342.
77 J. M. Van Raden, E. R. Darzi, L. N. Zakharov and R. Jasti, *Org. Biomol. Chem.*, 2016, **14**, 5721–5727.
78 D. Ari, E. Dureau, O. Jeannin, J. Rault-Berthelot, C. Poriel and C. Quinton, *Chem. Commun.*, 2023, **59**, 14835–14838.
79 V. Bliksted Roug Pedersen, T. W. Price, N. Kofod, L. N. Zakharov, B. W. Laursen, R. Jasti and M. Brøndsted Nielsen, *Chem. – Eur. J.*, 2024, **30**, e202303490.
80 T. C. Lovell, Z. R. Garrison and R. Jasti, *Angew. Chem., Int. Ed.*, 2020, **59**, 14363–14367.
81 Z. L. Qiu, C. Tang, X. R. Wang, Y. Y. Ju, K. S. Chu, Z. Y. Deng, H. Hou, Y. M. Liu and Y. Z. Tan, *Angew. Chem., Int. Ed.*, 2020, **59**, 20868–20872.
82 S. Nishigaki, M. Fukui, H. Sugiyama, H. Uekusa, S. Kawauchi, Y. Shibata and K. Tanaka, *Chem. – Eur. J.*, 2017, **23**, 7227–7231.
83 M. Ball, B. Fowler, P. Li, L. A. Joyce, F. Li, T. Liu, D. Paley, Y. Zhong, H. Li, S. Xiao, F. Ng, M. L. Steigerwald and C. Nuckolls, *J. Am. Chem. Soc.*, 2015, **137**, 9982–9987.
84 H. Thakellapalli, S. Li, B. Farajidizaji, N. N. Baughman, N. G. Akhmedov, B. V. Popp and K. K. Wang, *Org. Lett.*, 2017, **19**, 2674–2677.
85 T. Kuwabara, J. Orii, Y. Segawa and K. Itami, *Angew. Chem., Int. Ed.*, 2015, **54**, 9646–9649.
86 F. Lucas, J. Rault-Berthelot, C. Quinton and C. Poriel, *J. Mater. Chem. C*, 2022, **10**, 14000–14009.
87 P. Fang, Z. Cheng, W. Peng, J. Xu, X. Zhang, F. Zhang, G. Zhuang and P. Du, *Angew. Chem., Int. Ed.*, 2024, **63**, e202407078.
88 P. Seitz, M. Bhosale, L. Rzesny, A. Uhlmann, J. S. Wössner, R. Wessling and B. Esser, *Angew. Chem., Int. Ed.*, 2023, **62**, e202306184.
89 H. Ueno, T. Nishihara, Y. Segawa and K. Itami, *Angew. Chem.*, 2015, **127**, 3778–3782.
90 M. P. Alvarez, P. M. Burrezo, M. Kertesz, T. Iwamoto, S. Yamago, J. Xia, R. Jasti, J. T. L. Navarrete, M. Taravillo, V. G. Baonza and J. Casado, *Angew. Chem.*, 2014, **126**, 7153–7157.
91 Y. Xu, B. Wang, R. Kaur, M. B. Minameyer, M. Bothe, T. Drewello, D. M. Guldi and M. von Delius, *Angew. Chem., Int. Ed.*, 2018, **130**, 11723–11727.
92 Q. Huang, G. Zhuang, H. Jia, M. Qian, S. Cui, S. Yang and P. Du, *Angew. Chem., Int. Ed.*, 2019, **58**, 6244–6249.
93 Y. Tang, J. Li, P. Du, H. Zhang, C. Zheng, H. Lin, X. Du and S. Tao, *Org. Electron.*, 2020, **83**, 105747.
94 J. Zhang, L. Qiu, L. Liu, Y. Liu, P. Cui, F. Wang and Z. Zhang, *Nanomaterials*, 2022, **12**, 1408.
95 J. P. Mora-Fuentes, M. D. Codesal, M. Reale, C. M. Cruz, V. G. Jiménez, A. Sciortino, M. Cannas, F. Messina, V. Blanco and A. G. Campaña, *Angew. Chem.*, 2023, **135**, e202301356.
96 S. Z. Guo, L. Liu, L. S. Liu, Y. Q. Fan, H. J. Yang, J. He, Y. Wang, Z. S. Bo, X. J. Xu, X. B. Chen and H. Jiang, *ACS Appl. Mater. Interfaces*, 2025, **17**, 5202–5212.
97 C. Zhao, F. Liu, L. Feng, M. Nie, Y. Lu, J. Zhang, C. Wang and T. Wang, *Nanoscale*, 2021, **13**, 4880–4886.

